Physics – Uspekhi **67** (4) 361 – 378 (2024)

CONFERENCES AND SYMPOSIA

PACS numbers: **95.30. – k**, 98.70.Rz, 98.70.Sa

Sources of high-energy cosmic radiation

A M Bykov

DOI: https://doi.org/10.3367/UFNe.2023.04.039545

Contents

Abstract. The core collapse of massive stars and compact relativistic star mergers are accompanied by a rapid release of an enormous amount of energy, of the order of the rest energy of a star. Supernovae and gamma-ray bursts associated with these processes are observed almost every day by modern telescopes. Radiation from such sources is observed across the entire electromagnetic spectrum. Neutrinos from supernova 1987A and gravitational waves from relativistic star mergers have been detected. Along with rapidly variable and transient events, relativistic compact remnants of a collapsed star — accreting black holes and fast rotating pulsars — demonstrate high X-ray and gamma-ray luminosity for significantly longer times. The Crab Nebula and pulsars in gamma-ray binaries are excellent galactic laboratories that allow studying relativistic winds acting as cosmic high-energy particle accelerators. The study of physical processes leading to the conversion of the gravitational and rotational energy of relativistic objects into powerful electromagnetic radiation and high-energy neutrino fluxes provides unique opportunities for testing fundamental physical laws under extreme conditions unattainable in laboratory experiments on Earth. In this paper, we briefly review the results of observations and modeling of nonthermal processes in cosmic sources of high-energy radiation and discuss the prospects for advances in these studies.

Keywords: cosmic gamma-ray bursts, pulsar wind nebulae, gamma-ray binary sources, particle acceleration mechanisms, radiation processes in cosmic gamma-ray sources

A M Bykov
Ioffe Institute, Russian Academy of Sciences,
ul. Politekhnicheskaya 26, 194021 Saint Petersburg, Russian Federation
E-mail: byk@astro.ioffe.ru

Received 12 September 2023
Uspekhi Fizicheskikh Nauk **194** (4) 384 – 403 (2024)
Translated by S Alekseev

1. Introduction

Energetic processes in cosmic sources of X-ray, gamma, and neutrino radiation allow these sources to be observed up to cosmological distances. Gamma-ray bursts from collapsing stars have been detected up to redshifts $z \sim 9$, and there are prospects of detecting such events from early Population III stars. Within the general picture of the origin and evolution of powerful sources, the answers to a number of important questions remain obscure: questions both about the structure and mechanism of action of the central source of energy and momentum of a relativistic flow and about the properties of the flow itself, such as the plasma composition (relative fractions of baryons and $e^{\pm}$ pairs), the magnetization degree, the acceleration mechanism, and the structure of the anisotropic relativistic flow. To understand the causes of the high efficiency of conversion of the kinetic and magnetic flow energy into observable gamma radiation, particle acceleration and radiation mechanism models are needed. Observations of the spectra and light curves of gamma-ray bursts allow restricting the classes of such models and their parameters. Each of these problems is a subject of deep discussions in the literature. In this review, along with a brief discussion of the basic models, we focus on several recent results related to data obtained from multi-messenger observations of the unique gamma-ray burst GRB 220910A, as well as the detection of high-energy quanta in the TeV range by ground-based gamma-ray observatories to apply to the study of particle acceleration processes and radiation mechanisms. The physics of nonthermal processes in cosmic sources of hard radiation can be studied using observational data from galactic sources that are less powerful than gamma-ray bursts but are located closer. The relativistic winds of pulsars and microquasars provide us with examples of such sources. The possibility of long-term sensitive multi-messenger observations of a number of pulsar wind nebulae and binary gamma-ray sources with a spatially resolved structure of the emission region and measurements of radiation polarization in the X-ray range provides unique information on particle acceleration and emission of relativistic plasma flows. In what follows, we

discuss some recent research results concerning these objects.

Two decades of very successful operation of ground-based gamma-ray observatories have yielded interesting information about the high-energy emission from young supernova (SN) remnants, pulsar wind nebulae, active galactic nuclei, and some as yet unidentified cosmic sources of photons with energies above TeV. Such objects are mostly long lived, although they can exhibit rapid variability. Cherenkov telescopes of the ground-based observatories H.E.S.S., MAGIC, VERITAS, HAWC, LHAASO, TAIGA, and others, together with orbital gamma-ray and X-ray observatories and the MASTER global network of automatic telescopes, allow studying physical processes in sources of high-energy nonthermal radiation associated with supernova remnants, relativistic winds of pulsars, and jets of accreting black holes. These long-lived objects are observed in the Galaxy; in some cases, it is possible to study their spatial structure and detect quanta up to the PeV energy range. According to standard quantum electrodynamics models, the observation of PeV photons from cosmologically distant sources is impossible due to the large optical depth $\tau_{\gamma\gamma}$ arising due to the production of $e^{\pm}$ pairs by high-energy quanta on CMB photons. Therefore, observations of quanta with energies above 100 TeV from relativistic outflows of galactic objects, such as pulsar winds and jets from galactic black holes, provide unique information about the processes of particle acceleration and radiation at very high energies (we discuss some of them in Section 5), which allows a more thorough study of the physical processes of conversion of relativistic flows into radiation, gamma-ray bursts being an extreme example. Observing transient sources with detectors that have a limited field of view is not easy. Only recently did atmospheric Cherenkov telescopes first observe TeV-range photons from gamma-ray bursts GRB 180720B, GRB 190114C, GRB190829A, and GRB 220910A.

This review is a slightly extended version of a talk presented at the Scientific Session of the Physical Sciences Division of the Russian Academy of Sciences on April 21, 2023.

2. Gamma-ray bursts

2.1 Brightest sources of radiation in the Universe

Mysterious fast and bright bursts of cosmic gamma radiation were discovered 50 years ago [1, 2], but it took several decades to establish the cosmological nature of these events and associate them with relativistic stars. These most powerful sources of gamma radiation in the Universe are likely to be related to anisotropic relativistic outflows arising during the rapid accretion of matter onto a compact massive object. Such flows are formed, in particular, during the core collapse of a massive star or during the destruction of a neutron star in its merger with another relativistic star. At the sensitivity level of modern wide-field gamma-ray detectors such as Konus-Wind, Fermi/GBM, and Swift/BAT, gamma-ray bursts originating from random areas of the sky are detected approximately once a day. Tens of thousands of such events have already been detected, which has allowed determining a number of their important features and characteristics and constructing various models of the sources of these bursts. However, a number of significant problems in the physics of gamma-ray bursts remain unsolved; their discussion can be found, e.g., in reviews [3–8]. Gamma-ray bursts are a subject of numerous scientific publications: the complete review of publications on the subject from 1972 to 2010 in [9] contains more than 10,000 studies. We focus only on a few significant results, in our opinion, that have been obtained over the past few years. As an introduction, we first briefly describe the main observed characteristics of gamma-ray bursts and the ideas underlying the models of their sources.

The wealth of multi-messenger observations of gamma-ray bursts fits mainly into the framework of the model of a dissipative relativistic fireball formed due to the rapid release of energy (of the order of $M_{\odot}c^2$) of a collapsing relativistic object or a rapidly rotating magnetar, shown schematically in Fig. 1 (see, e.g., [10]). The observed high luminosity of gamma-ray bursts at cosmological distances, occasionally exceeding 10^{54} erg s^{-1} in isotropic equivalent [11], requires efficient conversion of the released energy into radiation. In the absence of a detailed model of bursts, their luminosity and released energy are characterized by the values assigned to an isotropic source. In fact, the radiation and ejecta are in many cases highly anisotropic, and the total energy release in the source can then be close to values typical of supernovae [12]. Recent observations of the afterglow of the most energetic gamma-ray burst known, GRB 221009A, indicate an anisotropic structured outflow [13]. The search for sources of multi-messenger afterglow in the absence of detection of the parent gamma-ray burst (so-called orphan GRBs) [14–16] should help determine the degree of ejecta anisotropy of the burst source and, very importantly, the fraction of supernova

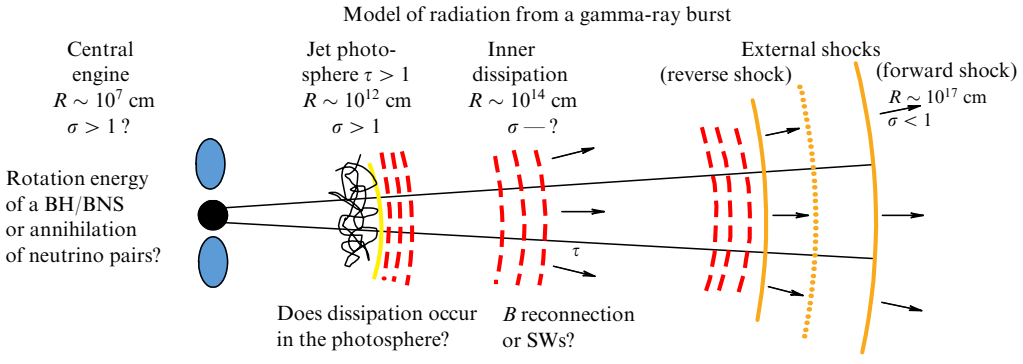

Figure 1. Sketch illustrating the discussed models of gamma-ray bursts based on idea of the formation of radiation observed during dissipation of relativistic outflow of a central engine [8, 10]. Source of powerful outflow is assumed to be due to rapid accretion of several $M_{\odot}$ of matter from collapsing stars onto a black hole or the formation of a rapidly rotating magnetar.

explosions with energetic relativistic ejecta. From the analysis of radio observations [14], the rate of bursts was estimated to be below 1000 per year in a region 1 gigaparsec (Gpc) in size. This is about a hundred times lower than the rate of supernovae associated with the collapse of massive stars (in particular, type Ib/c supernovae). Along with gamma-ray telescopes, the search for transient sources in the optical range is carried out by the Zwicky Transient Facility consortium (https://www.ztf.caltech.edu), the MASTER global robotic network for monitoring near and deep space (http://observ.pereplet.ru), and, in the X-ray range, the SPEKTR-RG orbital observatory [18]. In the near future, the search will be carried out in deep radio surveys by ASKAP (https://www.cadc-ccda.hia-iha.nrc-cnrc.gc.ca/en/racs/), the new Vera Rubin optical observatory (https://www.lsst.org/), and the ULTRASAT wide-angle orbital telescope in the near ultraviolet range [17].

Along with the very high energy, sources of gamma-ray bursts are characterized by a short duration of the prompt emission phase, measuring seconds, during which most of the energy is emitted, as well as by a strong variability of the flux at subsecond time intervals. Their observed spectra are also very unusual. The spectra of gamma-ray bursts can be characterized by the magnitude of the energy-differential photon flux F (measured in units of photon $\mathrm{cm}^{-2}\,\mathrm{s}^{-1}\,\mathrm{keV}^{-1}$), in the range from keV to tens of MeV and higher. The photon flux per unit energy interval, integrated over the entire time of the main burst (prompt), can frequently be approximately described by the empirical Band function [19], which is a piecewise power-law distribution $\mathcal{F}(E) \propto E^{-\alpha_{0,1}}$ with two exponents: α_0 for photon energies below E_p and α_1 for energies above E_p. The gamma-ray luminosity of the burst is $L_\gamma = \int E\mathcal{F}(E)\,\mathrm{d}E$. Because observations of bursts give $\alpha_0 \lesssim 1$ and $\alpha_1 > 2$, the energy flux of the prompt phase, $E^2\mathcal{F}$, is maximum for quanta with energy $E_\mathrm{p} \sim$ MeV. Observational data suggest an approximate dependence $E_\mathrm{p} \propto L_\gamma^{0.5}$, which allows estimating the cosmological redshifts of the sources [20, 21]. Band-type spectra are typical of gamma-ray bursts observed by the wide-field monitor detectors mentioned above. Observation of gamma-ray burst GRB 090902B (with redshift $z = 1.822$) by the Fermi/GBM monitor and the Fermi/LAT telescope allowed detecting several hundred photons with energies above 100 MeV during the prompt phase of the burst [22]. Importantly, a second spectral component was discovered in addition to the Band spectrum. The new component had an energy flux higher than that provided by the standard Band component for both photons with energies above 100 MeV and quanta with energies below 50 keV. High-energy quanta with energies above 100 MeV and a power-law energy distribution were recorded by the LAT telescope for more than 1000 s, i.e., for a much longer time than the duration of the prompt phase of the MeV burst. The presence of a second component during the main burst phase is a very important feature that must be explained by models of gamma-ray burst sources. Ten years after the discovery of the high-energy component of GRB 090902B, the ground-based Cherenkov telescope MAGIC detected GRB 190114C literally 50 s after the onset of the prompt burst [23, 24]. A similar gamma-ray telescope, H.E.S.S. (High Energy Stereoscopic System), detected an afterglow in the energy range of 100–440 GeV approximately 10 hours after the prompt phase of the very bright gamma-ray burst GRB 180720B ($z = 0.653$) [25]. The signal was recorded over several hours, demonstrating a decrease in the flux and in the maximum energy of the quanta. The H.E.S.S. telescope also recorded the afterglow of GRB 190829A in the time interval from 4 to 56 hours after the trigger, which allowed determining the photon spectral exponent as 2.07 ± 0.09 in the energy range of 0.18–3.3 TeV [26]. The measured gamma-ray spectrum and light curve of this burst are comparable to the characteristics of its X-ray emission, which is important for understanding the emission mechanism of such sources in the afterglow phase.

To elucidate the emission mechanisms of gamma-ray bursts, it is very important to analyze the photon spectra obtained with a time resolution that allows the contributions of individual pulses to be separated, and in the widest possible energy range. This has been done for the prompt phase of bursts [27–29]. Time-integrated spectra may not allow separating the contributions of different possible processes (see, e.g., [28, 30]). Below, we discuss significant deviations from Band's two-exponent empirical spectral model [31]. Emission during the prompt burst phase often exhibits rapid subsecond variability (tens of milliseconds). The time-integrated spectrum in the range of low photon energies $< E_\mathrm{p}$ often has a hard photon exponent $\alpha_0 < 2/3$. The photon exponent $2/3$ corresponds to the asymptotic spectrum of synchrotron radiation of monoenergetic particles (with a Lorentz factor $\gamma > 1$), in the frequency range below the characteristic peak $E_* \approx 0.29\gamma^2\hbar[3eB\sin(\theta)/2mc]$, where θ is the pitch angle of the particle [32].

The subsecond variability time of the observed gamma-ray emission indicates the compactness of the source, and its huge luminosity makes the presence of a relativistic flow of emitting particles with a Lorentz factor $\Gamma \gtrsim 100$ virtually inevitable in the source of the burst. This is due to the need to overcome the large optical depth of a compact source of quanta with energies above the electron–positron pair production threshold $\gamma\gamma \to \mathrm{e}^\pm$. For relativistic flows in a source with a redshift z, the optical depth is $\tau_{\gamma\gamma} \propto [\Gamma(1+z)]^{-(2\alpha_1+2)}$, where α_1 is the spectral exponent of the power-law distribution of the differential flux of photons ($F \propto E^{-\alpha_1}$) with energies higher than the energy E_p at which the energy flux of the prompt phase of the burst is maximum (see, e.g., [5]). The strong dependence of $\tau_{\gamma\gamma}$ on the Lorentz factor Γ of the flux in the radiation source at typical values $\alpha_1 \gtrsim 2$ allows solving the problem of radiation output from a compact source with $100 \lesssim \Gamma \lesssim 1000$. The characteristic radiation variability time $\tilde{t}_\mathrm{var}$ in the rest frame of a relativistic flow with a Lorentz factor Γ and dimensionless velocity β moving at an angle δ to the line of sight is converted in the observer's reference frame to $t_\mathrm{var} = \tilde{t}_\mathrm{var}/2\Gamma^2$ [5]. The observed time scales of variation in the radiation flux are of the order of 10 ms, which in the frame comoving with a $\Gamma > 100$ flow corresponds to the variability time $\tilde{t}_\mathrm{var} \sim R/c$; it is of the order of an hour and is determined by the source size R (before taking the redshift factor $1 + z$ into account in the observer's reference frame).

A compact central source with a rotating accreting black hole or neutron star (millisecond magnetar) forms a relativistic flow with a Lorentz factor Γ. In the isotropic case (relativistic wind), it can be conveniently characterized by its power

$$\dot{E} \approx 4\pi n_0 u \Gamma R^2 mc^3(1+\sigma)\,, \qquad (1)$$

where n_0 is the concentration of particles of mass m measured in the rest frame of the flow at a distance R from the center, and the radial 4-velocity of the flow u satisfies the equality

$u^2 + 1 = \Gamma^2$ [33]. The degree of magnetization of the flow is characterized by the parameter $\sigma = B_\perp^2/(4\pi\Gamma u n_0 m c^2)$, where the magnetic field component transverse to the flow velocity $B_\perp$ is measured in the laboratory frame. This definition is convenient for the flow of relativistic cold plasma to the wind stopping and heating surface, although more general definitions of the magnetization parameter are used in other problems. The approximate nature of equality (1) is related to the determination of the parameter σ in terms of the transverse field magnitude, which is convenient for relativistic flows. The characteristic size $r_\star$ of the region of energy release in the source is usually estimated as several hundred kilometers, which approximately corresponds to several radii of the innermost stable orbit of a Kerr black hole with a mass of the order of $10M_\odot$ or the radius of the light cylinder of a millisecond magnetar.

The dissipation of the kinetic and magnetic energy of the flow ensures the acceleration of particles and the formation of the light curve and emission spectrum of the source of a gamma-ray burst. Cosmological distances do not allow the source structure to be spatially resolved at early times of the main burst phase. During the afterglow phase, very long baseline radio interferometric observations were done for the very interesting short and close gamma-ray burst GW170817 (at a distance of about 41 kpc), with gravitational waves detected. The motion of radio components in the sky plane was detected with apparent superluminal velocities $v/c = 4.1 \pm 0.5$ [34] between 75 and 230 days after the burst. This allowed drawing important conclusions about the high degree of collimation of the relativistic flow and the lower bound for the Lorentz factor of the flow $\Gamma_0 > 10$ at the beginning of the afterglow phase. The gamma-ray burst GW170817/GRB 170817A belongs to the category of short gamma-ray bursts. Short bursts are conventionally defined as those with a duration up to 2 s and with hard spectra (see [7, 35, 36]). The origin of short gamma-ray bursts is associated with a huge release of energy during the merger of relativistic stars [37–39], which distinguishes them from long bursts associated with the core collapse of young massive stars in star-forming regions. The rate of relativistic star mergers accompanied by short gamma-ray bursts and emission of gravitational waves is determined by the nature of the evolution of compact binary systems [40]. Although the populations of short and long gamma-ray bursts are quite clearly separated [7], the example of GRB 211211A suggests some arbitrariness to that separation. This gamma-ray burst had a duration of 50 s, but observations of the afterglow indicate that it originated in a merger of relativistic stars [41]. The large amount of data on short gamma-ray bursts, including six-year observations of GW170817/GRB 170817A, requires a special discussion (see [42, 43]), which is beyond the scope of this brief review. However, we note recent optical observations of the source AT2017gfo/GW170817 in strong broad (P Cygni type) lines of strontium Sr^+ [44], which indicated a high degree of sphericity of the ejecta of the central source at early times. This circumstance is essential for modeling the so-called 'kilonovae,' which result from the merger of a neutron star and a black hole or another neutron star [45]. Kilonovae may result from a rapid merger, occurring in the last one or two revolutions of a binary system, of two neutron stars whose masses remain comparable until the instant of merger. In this case, the rapid rotation of the resulting collapsar can form a narrow relativistic jet. Another interesting scenario of the formation of kilonovae was proposed in [37]. It assumes a slow mass flow from one of the stars of the binary system to the other until the minimum stable mass of the neutron star (about $0.1M_\odot$) is reached, after which the star explodes, manifesting itself as a kilonova. Under the assumption of an initial imbalance between the masses of the merging neutron stars, such a scenario of the formation of fast-moving ejecta was considered, in particular, for GW170817/GRB 170817A [46]. Among long gamma-ray bursts, an interesting population of ultra-long gamma-ray bursts can be distinguished. For example, in the case of GRB 130925A, three episodes of high-energy emission with a duration of about 20,000 s were detected [47]. Also, an ultra-long burst GRB 220627A with redshift $z = 3.08$ has recently been discovered [48]. To explain the time interval between the two peaks of hard radiation observed in it, notably, a scenario is discussed in which the first peak is associated with the release of energy by a fast rotating magnetar and the second peak is associated with its collapse into a black hole [49].

The mechanism of the formation of a fast outflow depends on the nature of the source and the nature of the energy release. Several significantly different models of the central source of the burst have been proposed. A possible scenario is the formation of an optically thick region heated to relativistic temperatures during the core collapse of a massive star or a merger of stars, the expansion of the region being responsible for accelerating the plasma flow to significant Lorentz factors $\Gamma \gg 1$ [50, 51]. On the other hand, a relativistic jet with power $\dot{E} \propto a^2 \dot{M} c^2$ can be formed by a highly magnetized accretion disk surrounding a Kerr black hole with a dimensionless angular momentum a and a high matter accretion rate $\dot{M}$, formed during the collapse of massive stars (see, e.g., [52]). This scenario allows understanding the sharp cut-off in the power released by burst sources.

Magnetars — neutron stars with huge magnetic fields often exceeding the Schwinger field of quantum electrodynamics $B_{\rm cr} = 4.4 \times 10^{13}$ G — can form energetic outflows of magnetized plasma [53–55]. A magnetar that has a millisecond rotation period and an initially high magnetization $\sigma \gg 1$ can create a relativistic flow behind the light cylinder, where the electromagnetic field plays a dominant role, with the possibility of forming quite narrow (5 to 10 degrees) jets along its polar axis [56] and the subsequent conversion of the energy of these outflows into radiation. These and some other mechanisms of the formation of relativistic winds and jets are discussed in the literature as sources of energy for bursts and afterglows of various types. Of key importance are the flow geometry (collimation angle) and the value of the magnetization parameter σ, which determines the ratio of the fractions of energy flow transferred by the electromagnetic field and by the particles (see Eqn (1)). The ratio of the concentrations of baryons and leptons in the flow plasma also plays a very important role.

2.2 Dissipative relativistic flows of compact stars

The observed emission during the prompt phase of the burst is formed either at the boundary of the photosphere or in the inner dissipation region, directly behind the photosphere, which is defined as the region with optical depth $\tau > 1$ relative to Thomson photon scattering. The radius of the photosphere $R_{\rm ph}$ with $\tau = 1$ can be estimated as

$$R_{\rm ph} \approx \frac{\kappa \dot{M}_{\rm p} \sigma_{\rm T}}{4\pi \Gamma^2 m_{\rm p} c}\,, \tag{2}$$

where $\dot{M}_p$ is the proton injection rate (in terms of the isotropic equivalent), κ is the number of electrons and positrons per proton in the flow, and σ_T is the Thomson scattering cross section [51]. This gives the typical values $R_{ph} \gtrsim 10^{12}$ cm marked in Fig. 1.

The localization and mechanisms of energy dissipation of the relativistic flow differ significantly, depending on the fraction of baryons and the degree of plasma magnetization. When the fraction of baryons is small, depending on the value of the flow magnetization parameter σ, dissipation is likely to occur via rapid reconnection of magnetic fields of different polarities or in regions with small σ in collisionless shock waves (SWs). A significant part of the energy injected by the central engine can be converted into the observed radiation of the prompt burst both in the photosphere of the source through Comptonization of the photon field and in the inner dissipation region transparent to radiation, shown in Fig. 1 [57–60]. In flows that contain a significant fraction of baryons, collisional dissipation of the energy of protons and neutrons in the photosphere can help explain the observed hard emission spectrum exponents for photons with energies below E_p [61, 62]. Photospheric models allow reproducing the spectra of many gamma-ray bursts with photon emission indices $\alpha_0 < 0.5$ measured in the early phases of the prompt burst [63], a narrow frequency distribution of photons in the vicinity of the Band spectrum peak, and a relatively narrow interval of the observed peak energies. Models of dissipative photospheres with a magnetization parameter in the range of 0.001–0.1 can successfully reproduce the Band component in the spectra of gamma-ray bursts [59].

Inelastic collisions of protons and neutrons in dense regions of the photosphere allow naturally obtaining photons with energies of the order of $m_\pi c^2 \Gamma$ (where m_π is the π^0-meson mass) and are accompanied by the emission of neutrinos, which can be detected by IceCube [64], Baikal-GVD [65], and other observatories. For example, the spectra of the gamma-ray burst GRB 080916C [66] obtained with a sufficiently good time resolution are compatible with model predictions regarding the presence of a photospheric component in the radiation spectrum. The authors proposed an interpretation of the data in the framework of a multi-zone model of a relativistic flow coming from the central engine with a significant fraction of baryons but without strong plasma magnetization, and took both radiation from the photosphere and high-energy radiation caused by external SWs into account. At the same time, the analysis in [66] does not rule out a possible interpretation of the observations of GRB 080916C in the framework of other models.

The fundamental question of observational constraints on the fraction of baryons and the degree of plasma magnetization in sources of gamma-ray bursts has not yet been resolved, although there are some interesting results. For example, the interpretation of the ratio of the flux of TeV photons from bright GRB 221009A, detected by the LHAASO observatory during the prompt burst phase, to the flux of radiation from this event in the MeV range in the framework of the Compton scattering model of synchrotron MeV photons suggests the magnetization parameter in the relativistic flow $\sigma \gtrsim 1$ [67]. The authors discuss a model for the dissipation of the magnetic field of a flow in the form of multiple regions of field line reconnections with the formation of local minijets. The ratio of the energy densities of the magnetic field and the energy of particles (leptons and hadrons) in the vicinity of the central energy source up to the dissipation region is not determined by this method.

Along with photospheric models, scenarios with the dissipation of energy released by the central engine and the formation of the main gamma-ray burst in regions of the flow of optically thin plasma with $\tau < 1$ are possible. The rapidly varying release of source energy in the form of relativistically moving shells underlies a wide class of models with inner dissipation of the flow energy. In the reference frame of the central engine, two shells that left the central engine with a time separation Δt and move with different but comparable Lorentz factors (of the order of Γ) collide at a distance of the order of $R_{diss} \sim c\Delta t \Gamma^2$ from the engine and form a dissipation region there. Collisions of shells traveling with different speeds in the case of a weakly magnetized flow with $\sigma < 1$ should be accompanied by the formation of SWs, the acceleration of particles, and their nonthermal radiation (see Fig. 1). Models of radiation from a system of internal SWs are discussed in detail in [5, 50, 71–75]. Compton scattering of time-varying radiation from the photosphere by electrons and positrons accelerated by internal SWs can explain the emission component of the prompt burst with energies above 10 MeV (i.e., above the Band peak) [76]. This combined model assigns the MeV component of the Band spectrum to photospheric emission, and the more energetic emission of the prompt burst, to internal SWs.

An essential factor in assessing how realistic any given gamma-ray burst model can be is the efficiency of conversion of the central source energy into observable radiation and the ability to generate a photon spectrum that reproduces the observations. Indeed, the huge values of the isotropic equivalent of the energy release of gamma-ray bursts, even after correction for a high degree of radiation collimation [77] with collimation angles of several degrees, give the energy release of most gamma-ray bursts at a level of $\sim 10^{51}$ erg, which is comparable to the energy release during the collapse of a star. As a result, the model efficiency of conversion of the energy released by the central source into gamma radiation should be quite high.

In the simplest analysis of the energy of internal SWs in [5, 78], two nonmagnetized ($\sigma \ll 1$) shells are considered, with masses M_1 and M_2 and different velocities $\Gamma_1 > \Gamma_2 \gg 1$, merging into one with the Lorentz factor Γ_0. From the momentum and energy conservation laws, we have

$$\Gamma_0 \simeq \sqrt{\frac{M_1\Gamma_1 + M_2\Gamma_2}{M_1/\Gamma_1 + M_2/\Gamma_2}}. \quad (3)$$

When the shells collide and merge, part of their initial energy is released in the form of internal plasma energy. The ratio of internal energy to the initial total kinetic energy of the shells determines the conversion efficiency

$$\epsilon = 1 - \frac{(M_1 + M_2)\Gamma_0}{M_1\Gamma_1 + M_2\Gamma_2}. \quad (4)$$

As can be verified, the energy and momentum conservation laws allow a significant portion of the energy of kinetic shells to be converted into internal energy (and then into radiation) only for shells with a very significant difference in velocities $\Gamma_1 \gg \Gamma_2$, but with comparable masses. The estimates in [79] give an expected conversion efficiency of not greater than 20%. Energy efficiency is a very serious problem for models of internal SWs with a low degree of magnetization, even

when taking the Doppler effect and flow anisotropy into account.

The flow from a compact source of a gamma-ray burst can have a high degree of magnetization $\sigma \gg 1$ [57, 80–82]. In flows with a high magnetic field energy density, both photospheric dissipation and dissipation in the transparent region [60, 83, 84] are likely to be associated with the mechanisms of formation of current sheets in the regions of reconnection of magnetic field lines [54, 82, 85]. In the case of magnetized rapidly varying flows with $\sigma > 1$, the model of colliding shells considered above can be extended by including possible dissipation of their magnetic fields during the merger process [60, 83]. A simple model in which the magnetic dissipation rate is regarded as an external parameter allows obtaining an efficiency of tens of a percent only for systems with a rapid reconnection of field lines. A realistic determination of magnetic reconnection rates requires kinetic modeling of flows with magnetic fields of a complex structure in a wide dynamical range, starting from the scale specified by the dynamics of electrons [86–90]. We discuss the possibilities and some results of such modeling in the next section. We also note that the physical processes of dissipation of highly magnetized relativistic flows and the generation of accompanying nonthermal radiation can be studied using multimessenger observations of pulsar winds, discussed in Section 4 below.

2.3 Acceleration of particles in dissipative flows and their nonthermal radiation

To explain the observed spectra of gamma-ray bursts, blazars, and type-Ib/c supernovae, models of particle acceleration in dissipative relativistic flows must be used [72, 83, 91–94]. Particle acceleration mechanisms must ensure a sufficiently fast and efficient conversion of the energy of the relativistic flow into the energy of nonthermal particles at various phases of a gamma-ray burst [83, 91, 94–96]. In plasma flows with a moderate magnetization degree σ, particle acceleration can occur by the Fermi mechanism (in its various implementations). Acceleration of charged particles by nonrelativistic SWs and magnetic turbulence [97–102] is widely used to model cosmic ray sources in supernova remnants [103–107], but there are very important specific features of the particle acceleration process in relativistic plasma flows [108–110].

The formation of collisionless SWs and particle acceleration can be effectively studied by particle-in-cell (PiC) methods, implementing a self-consistent description of the kinetics of particles in electromagnetic fields [111]. Modeling the kinetics of particles and fields in planar relativistic plasma flows with different contents of baryons and magnetic fields was performed with the PiC TRISTAN code in [112–114]. The formation of collisionless SWs was observed when simulating flows with regular magnetic fields and a moderate magnetization degree $\sigma \leqslant 0.1$. The simulations in [114] showed that relativistic SWs propagating across a quasiuniform magnetic field effectively accelerate particles in a plasma of $e^{\pm}$ pairs if $\sigma \leqslant 10^{-3}$, and in electron–proton plasma with an even lower magnetization degree $\sigma \leqslant 3 \times 10^{-5}$. On the other hand, in flows with $\sigma > 10^{-3}$, acceleration of particles by SWs can occur if the magnetic field is nonuniform. A typical example of such a system is the equatorial relativistic wind of a pulsar, which can consist of alternating regions of high magnetic fields of different polarities. Computations in [115] showed that, in the region where such a wind stops, a plasma region with reconnection of magnetic fields and a termination shock is formed from $e^{\pm}$ pairs. In this region, rapid dissipative reconnection of magnetic fields and acceleration of particles occurs [115, 116]. When a magnetized relativistic wind is decelerated behind the termination shock front, a power-law distribution of accelerated particles is formed if the characteristic size of field regions of the same polarity is much greater than c/ω_p, where $\omega_p = \sqrt{4\pi n_0 e^2/\Gamma m_e}$ is the plasma frequency. The Fermi mechanism plays the main role in the formation of the spectrum of nonthermal particles behind the SW [116]. Acceleration of particles by perpendicular relativistic SWs is possible in a turbulent medium with noticeable average magnetization [96, 117, 118]. Both relativistic [119] and nonrelativistic shock waves can significantly enhance turbulent magnetic fields [120], which must be taken into account when modeling the afterglow of gamma-ray bursts.

PiC simulations of the dynamics of magnetic turbulence in a plasma of $e^{\pm}$ pairs with $\sigma \gg 1$ with a resolution of 2460^3 and with more than 10^{11} model particles [121–123] demonstrate the formation spectra of nonthermal particles and radiation. Recent studies of the kinetics of radiative plasma [122] approximately take the reaction force of synchrotron radiation into account, and PiC models taking Compton cooling of particles by an external radiation field into account are discussed in [124]. In systems with both source-driving turbulence [125] and decaying turbulence [126], particle acceleration has two phases. First, particles are injected from the thermal plasma by electric fields into magnetic reconnection regions; next, the energy of injected nonthermal particles increases due to stochastic acceleration on long-wave fluctuations by the Fermi mechanism [121, 125]. It is important that, due to the interaction of particles with current sheets, the angular distribution of nonthermal particles of relatively low energies is anisotropic, and the degree of anisotropy decreases as the energy increases [121, 122]. Synchrotron radiation spectra can be computed in the PiC model of the evolution of radiative relativistic plasma with an initial distribution of field fluctuations with $\sigma_0 \sim 50$ (in these computations, σ is the ratio of the magnetic energy to plasma energy density) [122]. In the low-energy range below the synchrotron peak, such spectra have photon indices $\alpha_0 \sim 1$, which is consistent with the observed spectra of the main phase of gamma-ray bursts. In the energy range above the synchrotron radiation peak, computations yield significant fluxes of photons with energies exceeding the so-called 'radiation reaction limit' (see also [127]). This is not surprising, because this model clearly shows the intermittent nature of magnetic turbulence with current layers and other magnetic structures. The possibility of overcoming the reaction limit of synchrotron radiation in systems with intermittent magnetic turbulence was previously demonstrated in models of giant Crab Nebula bursts [128, 129] (see Section 4 below).

Simulations with the PiC models are of course the most systematic ones and in many ways come close to a full-fledged numerical experiment. At the same time, simultaneous consideration of the injection and acceleration of the bulk of high-energy particles by the Fermi mechanism during interaction with long-wave fluctuations requires a large dynamical range of computations. High-resolution computations require considerable resources, which significantly limits the dynamical range of the simulation and implies a transition from microscopic plasma scales to hydrodynamic

ones. To rescale PiC models from microscopic scales, measured in inertial electron lengths c/ω_p, which are much smaller than the characteristic dimensions of emitting objects, combined models based on kinetic equations can be used. In particular, the processes of particle injection into a nonthermal population in the vicinity of current sheets in a plasma with a large σ or with SWs (in the case of moderate σ values) can be described on the basis of PiC models. Kinetic coefficients and source functions (particle injection rates) must be averaged over microscopic scales with the results obtained from the PiC computations taken into account. Three-dimensional PiC modeling of the decay of magnetic turbulence defined by the initial condition and the evolution of the distribution of particles in the plasma of $e^{\pm}$ pairs [126] in a cube of size $L \gtrsim 2000c/\omega_p$ showed that, in a time of the order of $10\,l/c$, where l is the energy-carrying scale of turbulence, most of the energy of magnetic fluctuations is transferred to particles to form their nonthermal distribution. In the framework of the considered model of the decay of magnetized plasma turbulence, the authors of [126] obtained the average rate of change in the energy of particles of a given energy and estimated the diffusion coefficient of particles in the particle energy space, characterized by their Lorentz factor γ:

$$D(\gamma) = \frac{\langle(\Delta\gamma)^2\rangle}{2\Delta t} \sim 0.1\sigma\left(\frac{c}{l}\right)\gamma^2. \quad (5)$$

In the simulations in [126], the time dependence of the parameters was determined by the evolution of the initial field distribution, but the dependence on the particle energy in (5) is due to the general properties of the interaction of particles with long-wavelength fluctuations [99]. Therefore, this dependence is probably suitable for an approximate kinetic description of systems with a source of energy of magnetic fluctuations and, further, for modeling particle spectra on hydrodynamic scales.

Kinetic equations for the distribution function of particles accelerated by the Fermi mechanism in systems with intermittent long-wavelength magnetohydrodynamic (MHD) turbulence and SWs, with particle energy losses taken into account, allow simulating the spectra of energetic particles [91, 130]. The kinetic coefficients used to calculate the particle spectra are expressed in terms of the statistical characteristics of turbulence: correlation functions of large-scale motions of plasma and SWs. The presence of intermittent non-Gaussian turbulence and multiple strong SWs in the system, or the possibility of a significant change in the particle energy over the fluctuation correlation length, characteristic of relativistic turbulence, requires going beyond the Fokker–Planck approximation and using integral equations inspired by the Kolmogorov–Feller equations [99, 131] and nondiffusion transfer processes with Lévy jumps [132].

Analyzing the time evolution of the spectra of gamma-ray bursts, the authors of [28, 31] found that their correct description is possible if a nonthermal power-law component with $\alpha_0 \sim 1.2$ is added to the blackbody component of the radiation, assuming that the acceleration of nonthermal $e^{\pm}$ pairs occurs in the radiating region of the flow. Previously, when studying a model of internal SWs with a synchrotron emission mechanism, the authors of [133] indicated that agreement with observational data required that only a small fraction of the flow particles responsible for radiation in the main phase of the burst be accelerated by the SW. This standard condition of the model of effective acceleration of pairs [91] was assumed to be satisfied in models of internal SWs [72, 73]. An analysis of the time evolution of gamma-ray burst spectra is needed to identify their emission mechanisms [27, 28, 134]. Emission spectra of the prompt bursts are observed in which, in the photon energy range below the E_p peak, the power-law index of the photon flux distribution changes from 2/3 to 3/2 (see, e.g., [135]). Models with fast synchrotron cooling of shock-accelerated particles naturally reproduce spectra with an index of 3/2, and hard spectra with a photon index of 2/3 are exhibited, e.g., by systems with a cutoff of the particle spectrum at a certain minimum energy [135]. A spectral cutoff at low energies does not correspond to models with fast synchrotron cooling of particles. Typical photon energies at which the transition from the hard index 2/3 to the index 3/2 occurs are estimated in [27] to be about 100 keV. If we interpret the change in the spectral index as a transition from the regime of fast synchrotron cooling of particles to a slow one, then, according to estimates in [27], the magnetic field in this region should be of the order of 10 G, which is several orders of magnitude less than the field expected in models of internal SWs with dissipation up to a distance of about 10^{14} cm from the central engine.

One of the advantages of models with fast cooling of particles is the high efficiency of the conversion of system energy into radiation [136]. To estimate the minimum required efficiency of the prompt burst, we can use the ratio of the radiation energy to the energy of the forward shock due to the interaction of the relativistic ejecta of the central engine with the environment [79, 137]. The ram pressure of the forward shock can be determined only by comparing models with the observed characteristics of the X-ray afterglow of bursts. A study of this problem in [79] showed that the minimum efficiency of the prompt burst in models of internal SWs can be reduced to a value $\sim 15\%$ instead of the much higher efficiency estimated previously in models with a large magnetic field in the main SW. The problem of energy efficiency of models with inner dissipation outside the photosphere remains unsolved [28], although unconventional approaches have been proposed, including the use of synchrotron emission of protons as the radiation mechanism in the prompt phase of the burst [135]. Previously, the authors of [138] discussed a model of the prompt phase of a burst with turbulent acceleration of particles in a plasma ejected by the central engine containing a mixture of baryons and leptons, in which secondary leptons resulting from inelastic hadron collisions yield hard spectra of MeV photons, but the second, GeV, component of the main burst can simultaneously be obtained. In the framework of PiC models with the emission of nonthermal $e^{\pm}$ pairs accelerated by magnetic turbulence, the authors of [121] demonstrated that an increase in the anisotropy of the angular distribution with a decrease in the particle energy allows obtaining hard spectra of synchrotron radiation. This provides possible ways for solving the problem of hard spectra during the prompt burst phase. One of the potentially important factors is the simultaneous consideration of particle acceleration and emission processes in nonstationary models of flow dissipation. This can extend the spectral models in [28] used to analyze the time evolution of the prompt burst.

In the simplest case, the kinetic equation for the time evolution of the isotropic part of the particle distribution function $N(p, t)$, with their acceleration by magnetic turbu-

lence in the region of flow dissipation and the energy loss due to radiation taken into account in the Fokker–Planck approximation, has the form

$$\frac{\partial N(p,t)}{\partial t}+\frac{\partial}{\partial p}\left[\dot{p}(p)N(p,t)-D(p)\,\frac{\partial}{\partial p}N(p,t)\right]+\frac{N(p,t)}{T_{\rm esc}}=\dot{Q}^{\rm inj}(p)\,, \tag{6}$$

where $\dot{p}(p)$ is the rate of particle momentum loss due to radiation, $D(p)$ is the diffusion coefficient in momentum space, and $\dot{Q}^{\rm inj}(p)$ is the rate of particle injection into the Fermi acceleration regime. This equation is written for the distribution function averaged over the volume of the system, and $T_{\rm esc}$ is the time it takes the particles to leave the acceleration region. The synchrotron radiation spectra for systems with large magnetization parameters σ in a relativistic flow were analyzed in [28, 31] based on stationary solutions of kinetic equation (6) for $e^{\pm}$ pairs, retaining only the term describing particle losses due to radiation $\dot{p}(p)$ and the external stationary source of accelerated particles $\dot{Q}^{\rm inj}(p)\sim p^{-\delta_{\rm p}}$ with a power-law distribution in a certain energy range. To correspond to observations, the spectral index of electrons in this model must be ~ 3.5, which differs from the standard index (~ 2.2) for the spectrum of particles accelerated by a relativistic SW in a low-magnetization system [28]. Most models of the emission spectra of a gamma-ray burst involved similar assumptions about quasi-stationary injection of the accelerated particles with a fixed index of the power-law distribution that corresponds to the case of rapid acceleration of particles in a strong SW. On the other hand, in models with effective acceleration of particles by magnetic turbulence, we can expect the spectrum of accelerated particles to evolve in time. In particular, in Fig. 2, we show the nonstationary spectra of particles in the case of acceleration by relativistic turbulence, obtained from solving Eqns (6) and (5) in the energy range where the rates of synchrotron and Compton losses of particles are lower than the acceleration time due to the Fermi mechanism. Such a range exists at relatively low energies, because the energy loss rate depends on the particle momentum $\propto\gamma^2$, and the rate of acceleration by long-wave magnetic turbulence changes more slowly. The isotropy approximation for the distribution function in the Fermi acceleration model at intermediate energies often turns out to be justified. Anisotropic distributions of particles in PiC models are realized at low energies, where particles are injected into the Fermi mechanism in the vicinity of current sheets of field line reconnection regions [121]. Figure 2 shows the evolution of the particle distribution from an injected narrow distribution at the onset of acceleration to broad, hard spectra of the particles accelerated by the Fermi mechanism on long-wavelength fluctuations with a subsequent decrease in intensity as the energy source is depleted. In this calculation, the particle injection source was stationary and monoenergetic, $\dot{Q}^{\rm inj}(p)\sim\delta(p-p_0)$ (with the number of accelerated particles varying with time). An estimate of the system acceleration time gave $T_{\rm a}\sim p^2/D(p)$. Taking the time evolution of the particle distribution function into account will allow comparing the observed spectra of gamma-ray bursts with a wider class of physical models than those considered in interesting study [28] using a stationary injection spectrum.

The question of the emission mechanisms of the main burst and afterglow continues to be the subject of extensive discussions [4, 57, 59, 79, 135, 139–141]. To reliably determine

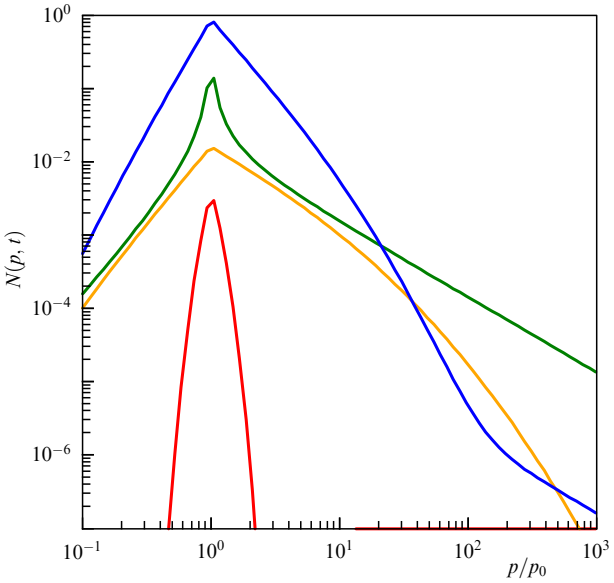

Figure 2. Time evolution of the model spectrum of particles accelerated by magnetic turbulence in a finite-size system with a characteristic particle escape time $T_{\rm esc}/T_{\rm a}=20$. Spectra of particles at time instants measured in the acceleration time units $T_{\rm a}$ are shown with color lines: 0.3 (red), 0.8 (yellow), 2.0 (green), and 12 (blue).

the emission mechanism, it is essential to have spectra of the main burst in a wide energy range (see [28, 142, 143]), together with time-resolved polarization data. Polarized radiation measurements are potentially very important both for establishing the radiation mechanism and for determining the properties of the flow [144]. In a number of cases, theories with a photospheric origin of the prompt burst predict a relatively low polarization degree of the radiation, not reaching 20% (see a review of the results in [144]). Models of the nonthermal component of the prompt burst that are based on the synchrotron emission mechanism in some cases predict a high degree of time-resolved linear polarization of radiation. An analysis of the time evolution of the position angle of polarized radiation can reveal the presence of substructures within the flow, such as minijets or magnetic pulses associated with internal SWs. Polarized radiation in the intervals between radiation pulses provides information about the global magnetic field of the relativistic flow.

Polarization observations of several bright gamma-ray bursts were carried out using the POLAR [145] and AstroSat [146] orbital detectors. In the bright gamma-ray burst GRB 160821A, the AstroSat detector [147] found evidence of a high degree of linear polarization, $66^{-27}_{+26}\%$ (with a 5.3σ significance estimate), in the energy range of 100–300 keV, with the position angle varying in time and changing significantly during the phase of increasing and decreasing intensity of the main burst. The authors of the observations concluded that the magnetic field is strongly ordered within the angles of $\sim 1/\Gamma$. The results of a joint analysis of data from observations of the gamma-ray burst GRB 170114A by the POLAR and Fermi/GBM orbital detectors [148] indicate a slow increase with time in the radiation polarization degree, reaching approximately 30% at the emission peak, which is consistent with the synchrotron model of the formation of the prompt burst. On the other hand, an analysis of 14 bursts detected by the POLAR instrument in the energy range of 50–500 keV [145] is indicative of little or no linear polarization of

radiation integrated over the burst time. To fully interpret the results obtained by AstroSat and POLAR, an independent analysis is needed of the bursts observed by both of these instruments, e.g., of the GRB 161218B burst, as is an analysis of the model of polarized emission from bursts [144, 149].

The literature also contains models of the polarization of radio and optical radiation in the afterglow phase [150], which take the presence of hydrodynamic-type turbulence ahead of the shock front into account. The authors of these models obtained an estimate of the polarization degree of $\sim 1\%$ for optical radiation and a slightly higher value for radio waves.

2.4 Lessons drawn from bright gamma-ray burst GRB 220910A

In most cases, powerful gamma-ray bursts have been observed from sources at redshifts $z \gtrsim 1$ due to the larger observed cosmological volume and the proximity to the time of maximum star formation rates. Therefore, the uniquely bright, relatively close gamma-ray burst GRB 220910A in a $z = 0.151$ galaxy (at a distance of about 745 Mpc) is a rare event, with an expected frequency of once per century or even less [13, 151]. The high integral radiation flux of GRB 220910A, ~ 0.2 erg cm^{-2} in the energy range of 20 keV–10 MeV [68], even caused disturbances in Earth's magnetosphere [152], observed from the propagation of low-frequency radio signals. In analyzing the radiation of this burst, the effects of galactic dust and the magnetic field of the Galactic disk had to be taken into account, because the source of the burst had a low galactic latitude of ~ 4.3 degrees. Observations of GRB 220910A were made across the entire range of the electromagnetic spectrum. Upper bounds for the neutrino fluxes from that source in the range from MeV to PeV were also obtained [153]. The JWST observations carried out 170 days after the event discovered a supernova remnant associated with GRB 221009A, similar to the previously studied object SN 1998bw. The amount of the ^{56}Ni isotope in the ejecta of the new SN residue, estimated as $\sim 0.09 M_\odot$, turned out to be very modest, and no spectral features indicating traces of the r-process of nucleosynthesis were detected. The host galaxy had a metallicity of about 0.12 of the solar one, and the star-forming region in which the source of the burst was located is unusual due to the presence in its spectrum of narrow lines of molecular hydrogen, previously detected only in one case, in the surrounding of the long gamma-ray burst GRB 031203 [154]. Estimates of the isotropic equivalent energy release of the GRB 220910A source based on observations in the range from 20 keV to 10 MeV exceed 3×10^{54} erg [13, 68, 155]. The light curve of the prompt phase of the burst contained several powerful pulses that occurred within approximately 600 s in the observer reference frame (see Fig. 3, taken from [68]), and the spectra of the radiation pulses were approximately described by the Band function with the indices $\alpha_0 \sim 1.1$ and $\alpha_1 \sim 2.6$, and a peak E_p of about 1 MeV.

A significantly new result was deduced in [156] from the analysis of data for the prompt phase of GRB 220910A detected with Fermi/GBM. The authors discovered a line in the emission spectrum with an energy of ~ 10 MeV and a width of about MeV, whose significance was estimated to be higher than 6σ. In the time interval of 280–300 s, a significant excess over the continuum model of two power-law components was discovered. The excess radiation was modeled by a Gaussian line centered at $12.56^{+0.3}_{-0.31}$ MeV with the width $1.31^{+0.3}_{-0.31}$. Then, within 80 s, the line center shifted from 12 to

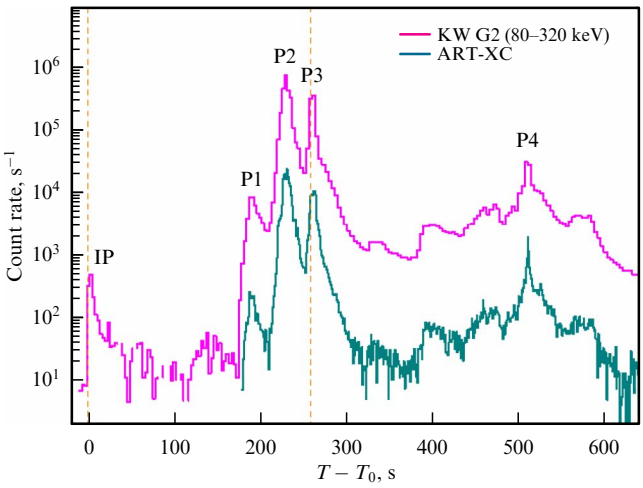

Figure 3. Light curve of uniquely bright gamma-ray burst GRB 221009A, measured by Konus-Wind detectors (Ioffe Physical-Technical Institute, Russian Academy of Sciences) and ART-XC (Space Research Institute, Russian Academy of Sciences) [68].

6 MeV, and the luminosity dropped from $\sim 10^{50}$ erg s^{-1} to $\sim 2 \times 10^{49}$ erg s^{-1}. Such a line can be interpreted as an $e^{\pm}$ annihilation line [157] blueshifted by a relativistic flow with a Lorentz factor $\Gamma \sim 20$, successively decreasing during the evolution of the burst [156]. In the framework of the internal SW model, the emission of the annihilation line can originate from a shell formed during a collision of a shell with a high Lorentz factor (> 100) with a slower shell at a distance of the order of 10^{15} cm from the central engine. Observations of emission and absorption lines in the gamma spectra of relativistic sources open up unique opportunities for testing models of such objects.

This result was obtained by analyzing a very bright burst, estimated to occur no more than once a century. Searching for lines from weaker bursts will be possible with more sensitive detectors. Figure 4 shows the minimum energy fluxes from cosmic sources that can be detected by some of the most sensitive X-ray and gamma-ray telescopes [69]. The figure illustrates the lack of sensitive orbital telescopes in the energy range around MeV. The area labeled ASTROMEV shows the

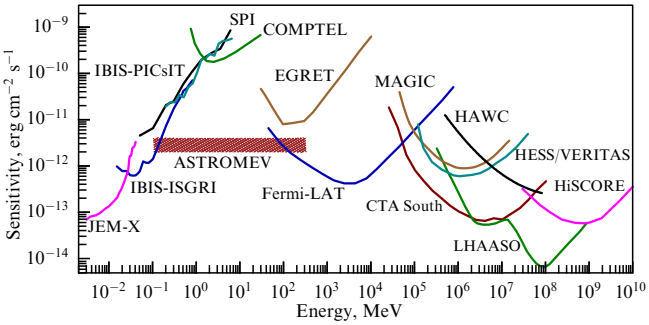

Figure 4. Sensitivity of some past, present, and planned gamma-ray telescopes. Characteristics of both orbital (recording photons up to energies of about 300 GeV) and ground-based Cherenkov observatories are shown [69]. Orbital detectors of gamma-ray bursts and other bright transients in the MeV range (Konus-Wind, Fermi/GBM, Swift/BAT, and Swift/XRT) have a sensitivity no better than 10^{-8} erg cm^{-2} s^{-1} and are not therefore shown. Planned sensitivity level of MeV-range Compton telescopes under development is designated as ASTROMEV.

achievable sensitivity of Compton telescopes that are currently being developed. The existing projects of orbital MeV observatories ASTROGAM [69], HERMES [158], COSI [159], and similar Compton detectors often have a slightly smaller field of view than do the wide-field monitors Konus-Wind, Fermi/GBM, Swift/BAT, and others, and therefore the expected number of gamma-ray bursts recorded by them will be fewer; however, even several high-sensitivity measurements of the spectra of bursts in the MeV range over several years of operation of these instruments in orbit will be highly informative. At the same time, designs of modern Compton telescopes with a wide field of view have also been proposed [160], which can be used to search for lines in the spectra of the main phase of a gamma-ray burst.

An analysis of the light curves of the afterglow of GRB 220910A in the infrared, optical, and X-ray ranges carried out in [161] showed that the observational data can be described by a model of synchrotron radiation from a forward shock of a highly collimated flow with a kinetic energy of the order of 4×10^{50} erg, propagating in a rarefied circumstellar medium formed by the wind of the progenitor star. However, explaining afterglow observations in the radio and millimeter ranges requires the introduction of additional components to the forward shock model. On the other hand, the authors of [13] showed that the data from multi-messenger observations of the afterglow both at the early moments and a month after the event do not fit into the model with a forward shock of a narrow collimated flow and are indicative of a structured flow. Notably, there is a possible contribution to the radiation from the reverse shock of a broader outflow propagating into a homogeneous interstellar medium. The considered possibility of dropping the assumption of the directivity of a narrow flow toward the observer will lead to a significant increase in the above estimate of the kinetic energy of the flow.

Observations of linearly polarized emission in the afterglow phase of GRB 220910A, carried out on October 11, 2022 by the IXPE orbital X-ray polarimeter in the energy range of 2–8 keV [162], set the upper limit for the polarization degree in the specified range at 13.8% (at a 99% confidence level). At the same time, due to the location of the burst close to the Galaxy plane, it was possible to observe the echo of this gamma-ray event in the form of a halo of X-ray photons scattered by the dust of the Galaxy. This allowed additionally imposing an upper bound on the degree of polarization of the soft X-ray emission of the main burst: 55% at a 99% confidence level. The authors concluded that the obtained bounds rule out the possibility that the source jet boundary is directed toward the detector but are consistent with models of the synchrotron mechanism for the formation of the prompt burst emission.

A very interesting feature of GRB 220910A was the observation of its emission in the TeV range [163–165]. Photons with energies above 10 TeV were detected from this nearby gamma-ray burst, which fortunately fell into the field of view of the LHAASO (Large High Altitude Air Shower Observatory) [165] and Carpet-2 gamma detector located at the Baksan Neutrino Observatory [164]. The first TeV photons were detected by LHAASO/WCDA a few minutes after the burst trigger, and more than 64 thousand photons with energies above 0.2 TeV were detected in just 50 min. The maximum fluxes of TeV photons were recorded approximately 10 s after the start of the signal, and the flux decay rate increased for approximately 10 min after the peak. The isotropic equivalent luminosity in the energy range of 0.3–5 TeV was 7.3×10^{50} erg s^{-1}, and the flux at the TeV radiation peak was 1.2×10^{-5} erg cm^{-2} s^{-1} [165]. Observational data are consistent with a model of a structured relativistic outflow with a half-width of the central cone of the order of 0.8 degrees [165]. This allows reconciling the very high estimate of the isotropic energy of the main burst dominated by MeV quanta, $\sim 10^{55}$ erg [13], with the theoretically expected energy release of the central source, $\sim 10^{51}$ erg. The detection of photons with energies above TeV indicates the action of effective processes of particle acceleration and subsequent emission, whose specific mechanisms have yet to be established [166, 167]. Of particular interest are detections of a photon with an energy ~ 18 TeV by the LHAASO observatory [163] and a photon with an energy of ~ 251 TeV by the Carpet-2 facility [164], announced in astronomical bulletins. Photons of such high energies should be thoroughly absorbed when propagating from a $z = 0.151$ source due to standard quantum electrodynamic processes (see, however, [166]). A possible explanation for the propagation of the high-energy quanta is related to their conversion into axion-like particles and subsequent reverse conversion into photons in the magnetic fields of galaxies [168, 169]. A model for the formation of the spectrum of high-energy radiation by a reverse shock during deceleration of a relativistic flow is discussed in [166]. In the time interval 300–400 s after the trigger, the spectrum of photons in the $\sim$GeV region, measured by the Fermi/LAT detector, was associated by the authors with Compton scattering of MeV photons from the prompt phase of the burst by accelerated electrons, along with the direct action of the synchrotron–Compton mechanism. The origin of photons with energies above $\sim$TeV in GRB 220910A ~ 600 s after the trigger is associated in [166] with synchrotron radiation of protons accelerated to ultra-high energies (also see [167]). During the period of emission of synchrotron photons in the TeV range by protons, the magnetic field energy density in the radiation region behind the reverse shock must have been large (up to half the flow energy density) [166], which indicates a high degree of magnetization of the initial flow. Similarly, from an analysis of the ratio of radiation energy fluxes in the TeV and MeV ranges ($\sim 2 \times 10^{-5}$), the authors of [67] deduce a high degree of magnetization of the relativistic flow in the radiation source.

The aggregate of observational data and the developed models do not yet provide an answer to essential questions about the physical processes occurring in the sources of gamma-ray bursts. The cosmological distance of these objects and the rapid decrease in luminosity at maximum brightness restrict the possibilities of observations. At the same time, the study of other types of powerful nonthermal sources can allow improving our understanding of the mechanisms of the formation of relativistic flows and particle acceleration and radiation. We briefly discuss new observations and models of some other types of transient sources.

Among powerful transient sources, soft repeating gamma-ray bursts (so-called repeaters) have traditionally been of particular interest. Since the discovery of the SGR 0525-66 burst in 1979 by the KONUS detectors from the Ioffe Physical-Technical Institute aboard the Venera 11 and Venera 12 spacecraft [170], the nature of 12 sources of repeating soft gamma-ray bursts has been confirmed to date, and several candidates are available. They are characterized by the release of $\gtrsim 10^{44}$ erg of energy in a fraction of

a second of the initial pulse, accompanied by a 'tail' of pulsating radiation that lasts hundreds of seconds. The main features of repeating bursts and their possible connection to the processes of energy release during rearrangements of the huge magnetic fields of magnetars were discussed in review [7]. In 2020, a connection was established between the burst of the soft gamma-ray repeater SGR J1935+2154 and the observed fast radio burst (see, e.g., [171]). This observation sheds light on the mystery of the nature of fast radio bursts [172, 173], which is of great interest, but the processes of formation of bursts in magnetars (see, e.g., [174, 175]) require a separate detailed discussion outside the scope of this paper.

3. Transient sources akin to gamma-ray bursts

After a short phase of the prompt burst with energy dissipation inside the relativistic outflow, further interaction of such a flow with the environment is accompanied by an afterglow phase that lasts several months. During the afterglow phase, particles are heated and accelerated by the external (forward) and internal (reverse) shocks, similarly to what happens during the interaction of a supernova ejecta with the circumstellar medium and is observed in supernova remnants [176]. In most supernova remnants, unlike gamma-ray bursts, the main energy of the burst is contained in the ejecta with a mass of the order of the solar mass, which therefore move predominantly at nonrelativistic speeds. In this case, only a small part of the flow kinetic energy E_k is in relativistic motions. Estimates of the distribution of kinetic energy over velocities for supernovae and gamma-ray bursts were made in [177]. Based on the hydrodynamic models studied in [178], it is convenient to parameterize the kinetic energy over the 4-velocities of external SWs $\Gamma_f\beta_f$ as $E_k(>\Gamma_f\beta_f) \propto (\Gamma_f\beta_f)^{-g}$. Data on remnants with nonrelativistic expansion rates of shells, which make up the vast majority of supernovae, are compatible with the estimate $g \sim 5.2$ of their exponent. Several relativistic supernova remnants without a gamma-ray burst, such as SN2009bb and SN2012ap, exhibit $g \gtrsim 2.5$, while $g \gtrsim 0.4$ in the case of gamma-ray bursts [177]. The physical nature of the energy distribution over 4-velocities can be associated with the characteristics of the central compact object (violent accretion onto a rotating compact object or the energy release of a millisecond magnetar). The authors of [179] demonstrated that, with the same total energy of 3×10^{51} erg ejected within different time intervals of 4.0, 7.5, and 15.0 s, it is possible to obtain $E_k(>\Gamma_f\beta_f)$ distributions with the g exponents ranging from 0.5 to 5.

The study of relativistic supernovae as an intermediate case between most supernova remnants and gamma-ray bursts allows us to better understand the processes of formation of the relativistic flow [180] and the mechanisms of particle acceleration to high energies [70, 181]. Based on very general arguments [92], without using a specific particle acceleration mechanism, it can be shown that transrelativistic plasma flows with $\beta\Gamma \sim 1$ and frozen-in turbulent magnetic fields are optimal for obtaining the maximum energy of accelerated particles at a given outflow power [70]. The expected (very uncertain) rate of relativistic supernova explosions in the Galaxy is approximately one event every 50 thousand years, which allows such objects to make a noticeable contribution to cosmic ray fluxes in the $\sim$ PeV energy range [182]. In Fig. 5, we show the spectra of protons accelerated by transrelativistic supernova SWs, computed

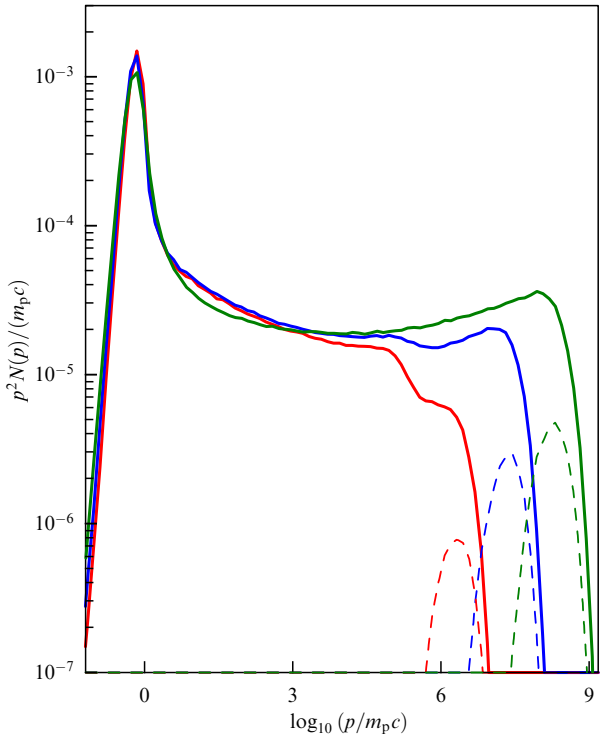

Figure 5. Energy distribution over spectrum of protons accelerated by a transrelativistic SW propagating at a speed of $0.3c$. Computations were performed for a planar SW within a nonlinear Monte Carlo model taking the effects of super-adiabatic amplification of magnetic turbulence by accelerated particles into account [70]. Spectra of particles for an SW propagating in the circumstellar medium with a magnetic field B_0 are shown by color lines: $B_0 = 3 \times 10^{-6}$ (red), $B_0 = 3 \times 10^{-5}$ (blue), and $B_0 = 3 \times 10^{-4}$ (green). Solid lines show spectra behind the shock front, and dashed lines show spectra of particles leaving the acceleration region into the interstellar medium.

within a nonlinear Monte Carlo model that takes the back reaction of accelerated particles on the structure of the wave and magnetic turbulence into account [70]. The spectra of protons depend on the magnetic field strength in the circumstellar medium, but protons accelerated to an energy of the order of PeV are present both inside the remnant and in the flow of particles leaving the acceleration region upstream from the SW. This apparently allows classifying relativistic supernovae as pevatrons—sources of cosmic rays with energies of $\sim$ PeV.

To understand the phenomena associated with the collapse of stars, several recently discovered rapidly variable objects, such as AT2018cow and AT2020xnd, called luminous fast blue optical transients (LFBOTs) [183–185], are of interest. These objects exhibit a rapid increase in optical emission within a day and a high luminosity reaching $\sim 10^{44}$ erg s^{-1} at the peak and decreasing over the course of several weeks. A rapid expansion of the radio source with moderately relativistic speeds of $\gtrsim 0.1c$ is observed, possibly initiated by a relativistic jet from the central source, which did not pass through the dense shell of the SN progenitor star without significant modification. The interaction of the jet with the stellar envelope can form an anisotropic structure, a so-called cocoon, expanding at a speed of the order of $0.1c$, ahead of the more massive SN ejecta, which has a speed $\sim 0.01c$. Observations of the vicinity of the AT2018cow source, located at a distance of $\gtrsim 60$ Mpc, with the ALMA,

VLT/MUSE, and HST/WFC3 instruments [186] revealed a cloud of molecular hydrogen with a total mass of $\sim 6 \times 10^6 M_\odot$ and two star-formation regions with total masses of stars of $\sim 3 \times 10^5 M_\odot$ each. The authors of the observations believe that the AT2018cow source is located closer to the line of sight than these objects, and suggest that its progenitor was about 10 million years old and had a mass of less than $20 M_\odot$. This conclusion was based on the absence of a visible population of young stars directly around AT2018cow, which allows attributing its origin to earlier episodes of star formation in this region, comparable in characteristics to the star formation region 30 Dor located in the Large Magellanic Cloud. Available observations so far have provided only very limited information about the nature of these interesting sources, in particular, about nonthermal processes of particle acceleration and their high-energy radiation, but studies of such objects are just beginning. The search for and observations of bright transient sources will be the purpose of the wide-field (204 square degrees) ultraviolet telescope ULTRASAT (ultraviolet transient astronomy satellite), whose launch is planned for 2026 [17]. The Russian Spectr-UV observatory [187] will allow both gamma transient studies with KONUS detectors and UV spectroscopy of the afterglow regions.

Essential information about the physics of nonthermal processes that ensure the conversion of the power of relativistic plasma flows into high-energy radiation can also be obtained by studying pulsar wind nebulae. Dozens of such objects are observed in our Galaxy, and their relative proximity in some cases allows studying the spatial structure of the relativistic wind and synchrotron nebulae formed after the relativistic plasma flow has stopped. In what follows, as an example, we discuss the gamma-ray emission from the Crab Nebula, which has a very high efficiency of converting pulsar spin-down power into pulsar wind and nonthermal radiation.

4. Variable gamma radiation from the Crab Nebula

Relativistic winds from energetic pulsars are observed across the entire range of the electromagnetic spectrum in the form of extended synchrotron nebulae (the Crab Nebula is a prototype of such an object) and are therefore natural laboratories that allow studying the processes of particle acceleration and the formation of radiation from magnetized flows [33, 127, 188]. The Crab Nebula is observed in a photon energy range spanning 22 decades, from the radio to gamma-ray range. The main models of pulsar wind nebulae imply the conversion of a significant portion of the power released due to the pulsar rotation braking into an anisotropic wind of electrons and positrons, with a possible admixture of protons, with a high value of magnetization σ and the Lorentz factor $\Gamma \gg 1$. The wind termination upon collision with the environment is accompanied by processes of particle acceleration to high energies. Synchrotron radiation determines the spectrum ranging from radio waves to gamma rays with energies up to GeV, and inverse Compton scattering of photons by electrons accelerated to PeV forms a spectrum of radiation energies above GeV.

The problem of accelerating a pulsar wind propagating behind a light cylinder [189, 190] has not yet been fully solved, but useful approaches to modeling axisymmetric flows have been developed [191]. A significant fraction of the power of the relativistic wind is concentrated in the vicinity of the equatorial plane of the pulsar [192, 193] and is released in the vicinity of the wind termination surface [127]. In the models, a high degree of magnetization of the relativistic wind $\sigma \gg 1$ is assumed in the vicinity of the light cylinder, while the formation of the termination shock requires a significant decrease in σ. In the model of a tilted magnetic rotator, the structure of the pulsar wind near the light cylinder can consist of stripes of a toroidal field with variable polarity [189]. In the region where the wind stops, the processes of reconnection of magnetic fields of different polarities can lead to a significant reduction in the magnetization of the plasma and to the termination shock formation [115, 116]. Computations performed by these authors using the PiC method demonstrated the effective acceleration of particles by electric fields during the dissipation of magnetic fields, as well as acceleration by the Fermi mechanism in the vicinity of the SW. Electrons and positrons accelerated in the wind termination surface emit synchrotron radiation, observed as a pulsar wind nebula in various ranges of the electromagnetic spectrum. The structure of magnetic fields behind the region where the relativistic wind of a pulsar stops plays an important role in the formation of the observed synchrotron nebula, whose shape depends on the angle of inclination of the rotation axis to the magnetic dipole of the pulsar [194], as well as on the properties and motion of the medium surrounding the pulsar [195]. X-ray observations carried out with high angular resolution by the Chandra telescope [188, 196–198] revealed a remarkable diversity of shapes and spectra of pulsar nebulae. The efficiency of conversion of the relativistic pulsar wind power into observable nonthermal radiation also varies greatly in such objects. In the Crab Nebula, this efficiency reaches several percent, but in most nebulae it is several orders of magnitude lower.

The powerful gamma-ray flares from the Crab Nebula discovered by the orbital observatories AGILE [199] and Fermi [200] are of considerable interest for understanding the nature of high-energy radiation. The Crab Nebula is generally regarded as a fairly stable source of hard radiation with photon energies above keV and is used to calibrate many detectors. Therefore, the discovery of gamma-ray flares of the order of several hours in duration with an increase in the flux of photons with energies above 100 MeV by more than an order of magnitude turned out to be a big surprise for researchers [201]. The emission power of strong GeV bursts exceeded 10^{36} erg s^{-1}, which is about a percent of the Crab pulsar spin-down power. Longer and lower amplitude variations in the gamma-ray flux from this nebula were also detected, and finally long (several weeks) periods of strong decreases in the observed gamma-ray flux were detected, as shown in Fig. 6 [202]. An important feature of the strong variations in the Crab Nebula emission is that the variability is restricted to the photon energy range from approximately 100 MeV to several GeV, corresponding to the cutoff range of the synchrotron radiation spectrum. A simultaneous search for flux variability in all other (including TeV) energy ranges did not reveal significant deviations from the stationary value [201, 203]. A significant problem that arises in interpreting such flares is also that the peak emission of the burst occurred at energies above 100 MeV. In single-zone models with electron acceleration by the Fermi mechanism by MHD SWs and simultaneous synchrotron radiation, the maximum energy of the emitted photons should not be much greater than $m_e c^2/\alpha_f$, where α_f is the fine structure constant [204]. The

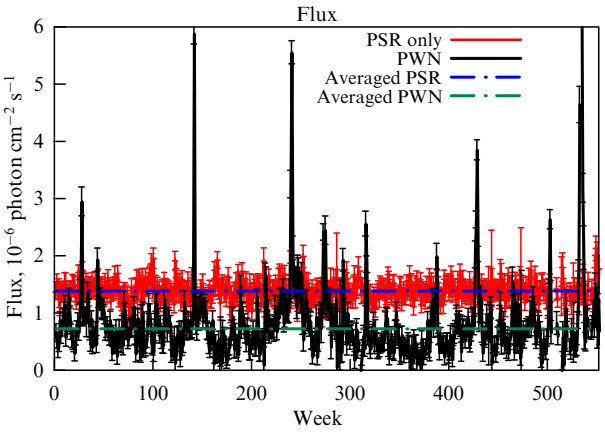

Figure 6. Light curves of the Crab pulsar (red line) and the Crab Nebula (black solid line) in photon energy range of 100–300 MeV detected during 10.5 years of measurements by the Fermi LAT telescope [202]. Clearly seen are strong gamma-ray flares and significant periods of depression of radiation flux (of varying durations) relative to average value of gamma-ray flux, shown by green dashed-dotted line.

condition that the magnetic field is frozen into the plasma does not allow obtaining electric fields with a strength higher than magnetic ones in ideal MHD models. Violation of the frozen-in condition in the vicinity of current sheets during magnetic reconnection removes this restriction. Models of fast magnetic field reconnection have therefore been proposed that allow accelerating electrons to energies of the PeV regime with a synchrotron radiation spectrum similar in shape to the emission spectrum of a single particle and a peak at energies above 100 MeV [205]. On the other hand, radiation from synchrotron quanta with energies above 100 MeV can also be obtained in an ideal MHD system where particle acceleration and radiation regions are separated in space or time, i.e., in systems with strong magnetic field fluctuations [128, 129]. Magnetic field fluctuations lead to very strong variations in the flux in the region of the synchrotron radiation spectrum cutoff and have a much lower effect on the fluxes of lower-energy photons, which corresponds to the existing observational constraints [128]. If the emitting plasma moves with a relativistic speed toward the observer, then the energy constraints of the single-zone MHD model can be easily overcome, which was discussed in [203]. The termination surface of the relativistic wind has segments with oblique SWs, the plasma motion behind which can have moderate relativistic Lorentz factors of the order of several units. Localization of the flare source in a region moving with a characteristic Lorentz factor $\Gamma \sim 3$ downstream behind the front of a tilted termination shock allows explaining the short observed duration of the burst and relaxing the energy requirements for MHD models with field fluctuations. Models of extreme particle acceleration in the magnetic reconnection regions can explain observed gamma-ray flares. However, the light curve of the Crab Nebula in the photon energy range of 100–300 MeV [202], shown in Fig. 6 with a black solid line, clearly demonstrates both the flaring activity and significant periods of depression of various durations (the dashed green line shows the average flow). Both the flaring activity [199, 200] and periods of strong depression of the radiation flux in the range of 100–300 MeV discovered in more than 10 years of data from the Fermi telescope [202] are naturally explained in MHD models with highly fluctuating magnetic fields if, due to strong synchrotron losses of electrons, the emission region of gamma rays is localized in a narrow moderately relativistic flow behind the termination shock front of the pulsar wind.

No flaring activity in the Crab Nebula above GeV has been detected to date. Gamma-ray emission from the Crab Nebula at energies above GeV is mainly due to Compton scattering of the photon field by ultrarelativistic electrons and positrons with a possible contribution from hadronic processes [206]. The study of the possible contribution of PeV proton emission to the observed fluxes of photons with energies above 100 TeV from the Crab Nebula is of great interest, because the question of the fraction of baryons in the relativistic wind of a pulsar remains open. Long-term observations of the flux of PeV photons from the Crab Nebula by the LHAASO and TAIGA gamma-ray observatories [207] will allow clarifying the question of the presence of a spectral component due to PeV hadrons. Also possible is acceleration of the environment protons in the region where the pulsar wind stops. In this regard, we discuss recent observations of photons with energies above 300 TeV from the Cygnus region by the Carpet-2 installation.

5. Relativistic stars in binary gamma-ray sources as petaelectronvolt particle accelerators

Detectors of Carpet-2, a complex installation for observing extensive air showers at the Baksan Neutrino Observatory of the Institute for Nuclear research, Russian Academy of Sciences, discovered a probable (with approximately 3σ significance) excess of photon events with energies above 300 TeV from the region of the Galaxy called the Cygnus Cocoon; this excess can be interpreted as a gamma-ray flare [208]. The presumed flare had a duration of about 82 days, the flux of quanta with energies above 300 TeV was determined as $(5.6 \pm 1.8) \times 10^{-12}$ photons cm^{-2} s^{-1}, and the time-integrated flux was $\sim 13 \pm 4$ GeV cm^{-2}. It is important that the registration of this flare coincided in time with the neutrino event IceCube 201120A. The photon radiation energy flux recorded by the Carpet-2 installation was very high, which was not predicted by the existing models of gamma radiation from clusters of massive stars located in the Cygnus region. Independent confirmation of the significance of detecting this flare by other observatories has not yet been obtained, and the likelihood of a repeat event of this type depends on possible models of the source, which we discuss below.

The region of the Galaxy in the direction of the constellation Cygnus is rich in clusters of young stars and sources of high-energy radiation [210–213]. In particular, quanta with energies up to 1.4 PeV were recorded from the source LHAASO J2032+4102 [214] in the Cygnus Cocoon region, which was discovered as an extended source of gamma radiation [209, 215]. Figure 7 shows a GeV image of the Cygnus Cocoon obtained from Fermi observations [209]. This extended radiation source is tens of parsecs in size at the distance of ~ 1.5 kpc of the cluster of young stars in Cygnus. This image also shows the positions of the massive star cluster Cyg OB2, the supernova remnant Gamma Cygni, and the binary gamma-ray source PSR J2032+4127/MT91 213. Clusters of young massive stars Cyg OB1, Cyg OB2, and others are probable particle accelerators [216] and sources of high-energy gamma radiation [217, 218]. However, the short characteristic flare time and the high flux of radiation detected by the Carpet-2 installation with energies exceeding 300 TeV do not correspond to those expected from extended

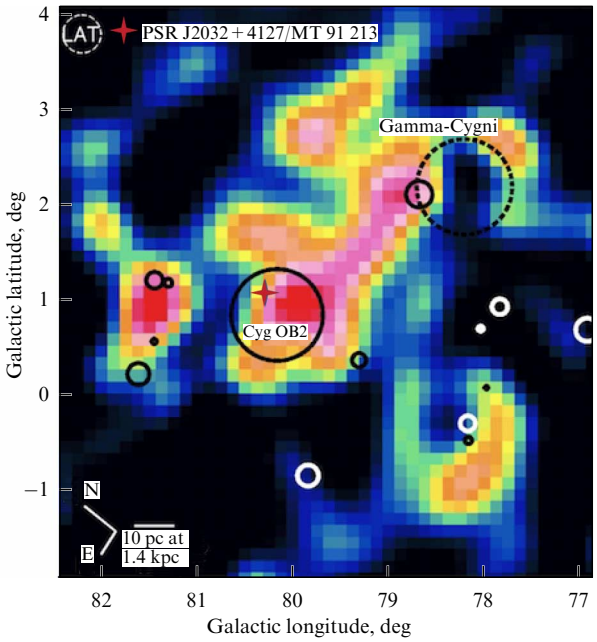

Figure 7. Image of the Cocoon Cygnus gamma-ray source in the GeV photon range according to observations by the Fermi observatory [209]. Also shown are positions of young massive star cluster Cyg OB2 (solid ring), supernova remnant Gamma Cygni (dashed ring), and binary gamma-ray source PSR J2032+4127/MT91 213 (red cross inside solid ring).

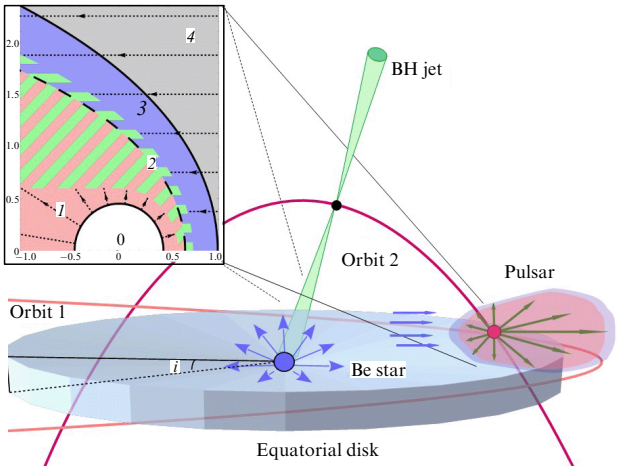

Figure 8. Schematic illustration of the interaction of the wind of a massive star with the relativistic wind of a pulsar whose orbit is labeled Orbit 1. Another possible scenario for a high-energy gamma-ray source is illustrated by a black hole with a jet moving in Orbit 2 in a close binary system including a massive star (for example, Cyg X-3). Inset shows structures included in model computations of the spectrum of relativistic protons: termination shock of relativistic pulsar wind, bow shock stopping the wind of a massive star, and contact region between them (blue) [225]. Model proton spectra calculated by the Monte Carlo technique are shown in Fig. 9.

structures larger than a parsec in size. Compact objects in binary gamma-ray sources observed in the Cygnus Cocoon region, Cyg X-3 [219] and the pulsar in the Be star binary system PSR 2032+4127/MT91 213, are certainly interesting candidates. Cyg X-3 is a binary system with a period of ~ 4.8 hours located at a distance of $\gtrsim 7$ kpc, whose components are a compact relativistic object (black hole or neutron star) and a massive Wolf–Rayet star. Microquasar Cyg X-3 exhibits rapidly varying emission in various ranges [220, 221] and has a one-side jet [222]. The possible role of the microquasar Cyg X-3 as a source of neutrinos recorded by the IceCube observatory was recently discussed in [223]. However, the Cherenkov telescopes MAGIC and VERITAS set only upper bounds for Cyg X-3 radiation above 250 GeV at the level of $\gtrsim 10^{-12}$ photons cm^{-2} s^{-1} [212, 224] at various periods observations, including during radio flares and gamma-ray flares in the GeV range. The short orbital period and upper bounds on teraelectronvolt radiation make the explanation of the nearly three-month duration of the 300-TeV radiation burst somewhat less natural, but Cyg X-3 nevertheless remains a possible candidate source of this radiation.

The binary gamma-ray source PSR J2032+4127/MT91 213 located at a distance of ~ 1.4 kpc has a long orbital period of about 50 years (periastron was probably passed in 2017). The pulsar rotation period is ~ 143 ms, and the spin-down power is estimated as $\dot{E}_r \sim 2 \times 10^{35}$ erg s^{-1} [226]. We note that this power is close to the isotropic equivalent of the flare luminosity measured by Carpet-2 if the source was located at the distance of the pulsar. Multiwave models of PSR J2032+4127/MT91 213 radiation [227] allow explaining the observed fluxes of quasistationary radiation, including gamma radiation in the TeV range at the level of $\lesssim 10^{-12}$ erg cm^{-2} s^{-1}, measured by the MAGIC and VERITAS telescopes near the periastron of the orbit [228]. The radiation energy flux according to Carpet-2 data is several orders of magnitude higher, which requires a modification of the models if association of this burst with the PSR J2032+4127/MT91 213 binary system is attempted. Potentially, radiation fluxes from this object above 100 TeV can be obtained at the level of $\gtrsim 10^{-10}$ erg cm^{-2} s^{-1} if there is a particle acceleration mechanism that gives rise to a hard spectrum of protons $N(p) \propto p^{-s}$ with an exponent $s \gtrsim 1$, extending from energies $\gtrsim$ TeV to values much higher than PeV. In this case, photons with $\gtrsim 300$-TeV energies and the accompanying neutrinos can be obtained due to the threshold-type photomeson radiation of the accelerated protons interacting with the powerful optical radiation of the bright Be star MT91 213. Such a model was proposed in [225]. In Fig. 8, which illustrates the possible scenarios, in particular, we show the collision region of the relativistic wind of the pulsar with the fast wind of the Be star. Simulations of the transport and acceleration of ultrarelativistic protons in the collision region of stellar winds (shown in the inset to Fig. 8), carrying magnetic fluctuations that resonantly scatter relativistic particles, were performed using the Monte Carlo technique. The possibility of forming very hard spectra of protons in the PeV range has been demonstrated if protons are preaccelerated to energies of the order of TeV in single SWs. An example of the computation of such a spectrum of protons accelerated in a system with a strongly magnetized stellar wind is shown in Fig. 9, and the corresponding spectra of photomeson radiation are represented by solid green (neutrinos) and blue (photons) lines in Fig. 10. This figure shows only model emission spectra of protons accelerated during the flare phase to energies above PeV in the region of wind collision. A significant contribution to the observed quasistationary photon emission in the GeV–TeV energy range is made by the emission of relativistic electrons and positrons, the modeling of which is discussed in [227].

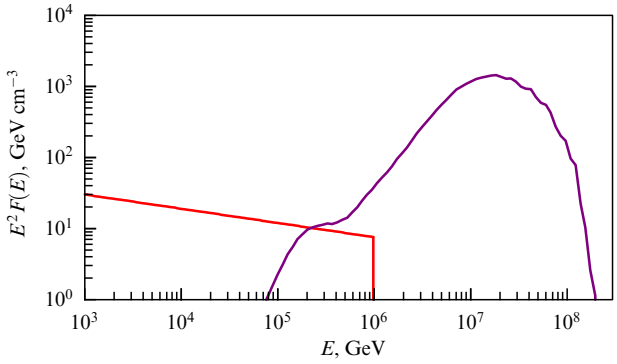

Figure 9. Model spectrum of protons accelerated in the region of collision of winds of a pulsar and a massive star [225]. Computation was performed using Monte Carlo technique for region whose structure is shown in the inset to Fig. 8. Spectrum of protons preaccelerated by a single SW in the system is shown with the red line. In second phase of acceleration, these protons with energies of $\sim$ 100 TeV are injected into acceleration process by the Fermi mechanism in plasma flows of colliding winds of the pulsar and the star, forming a hard spectrum of particles extending to energies above PeV. Spectrum of protons accelerated in second phase is shown with solid purple line.

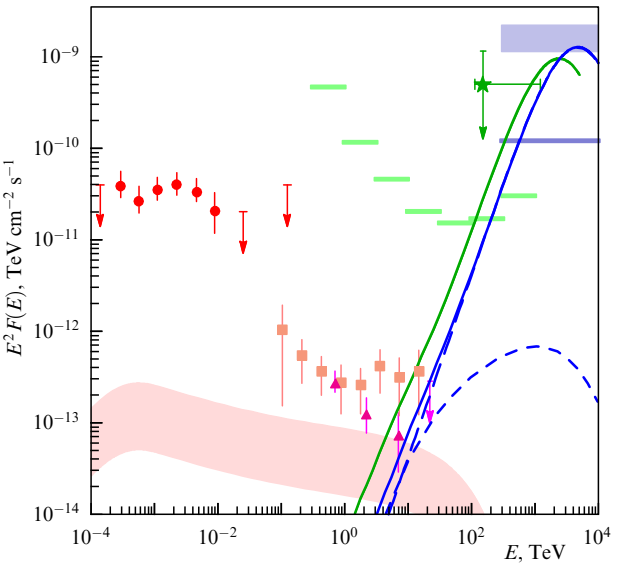

Figure 10. Model spectrum of photomeson radiation from PeV protons (see Fig. 9) accelerated in the region of collision of winds of a pulsar and a massive star is shown by solid green (neutrinos) and blue (photons) lines [225]. Photomeson gamma radiation is caused by collisions of ultrarelativistic protons that have overcome the reaction threshold with optical quanta from a hot massive star. The fluxes detected by Carpet-2 facility during the flare [208] are shown with purple area, and flux estimate for IceCube 201120A neutrino event is shown with green star. The range of radiation fluxes expected in the model from inelastic proton–proton collisions of accelerated particles with surrounding plasma is marked in pink. Being summed with photons from inverse Compton scattering (models of GeV–TeV lepton emission not shown in the figure), they can explain TeV observations by Cherenkov telescopes, marked with filled red squares and triangles. Fermi telescope data (red dots) can be described by the radiation of relativistic leptons [227].

We note that the nonthermal X-ray spectrum of PSR J2032+4127/MT91 213 observed by the Chandra and NuSTAR telescopes became much harder (with the photon index of the power spectrum α_0 changed from 2 to 1.2) in the periastron of the orbit [229]. Nonthermal X-ray emission is likely due to synchrotron emission from relativistic electrons and positrons [227]. In this case, the spectrum of particles accelerated in a binary system should also be hard, with the main share of energy carried by particles close to the cut-off) of the hard component, which for relativistic $e^{\pm}$ is determined by synchrotron/Compton energy losses. The synchrotron spectrum maximum should be around MeV in this case, and its position would then provide significant information about the properties of the system. Measurements in this region require new Compton detectors with the sensitivity discussed in Section 2.4 and shown as the ASTROMEV level in Fig. 4. The possibility of forming very hard spectra in which particles with maximum energies contain most of the energy density of nonthermal components is related to the presence of magnetically fluctuating colliding plasma flows in the system. In colliding MHD flows of turbulent plasma, a version of Fermi acceleration can be implemented [216, 230], such that the resulting spectra are harder than in the case of diffusive acceleration of particles by single SWs.

An important issue to be discussed regarding the applicability of the PSR J2032+4127/MT91 213 model to explaining the Cygnus flare is the energetics of the system. The available power of the binary gamma-ray source PSR J2032+4127/MT91 213 corresponds by order of magnitude to the pulsar rotation deceleration power $\dot{E}_r$, which is comparable to the gamma-ray luminosity of the system in the isotropic equivalent during the flare detected by Carpet-2 installation. Within the model, this suggests a possible anisotropy of the radiation. Hard spectra of protons and radiation in Figs 9 and 10 were obtained in [225] for a pulsar moving through the wind of a massive star with a strong magnetic field $\sim$ Gauss at a distance of the order of several astronomical units from the star. This implies a magnetic field strength above 100 G on the surface of the star, which does not contradict the statistics on the observed fields of massive stars. To clarify the problem of possible anisotropy of gamma radiation, models of the evolution of a pulsar wind colliding with the magnetized wind plasma of a massive star have been constructed.

In Fig. 11, we show a simulated model of the interaction region of the relativistic wind from a pulsar with the fast wind of a massive star carrying a magnetic field of $\sim$ 1 G. The presence of a strong magnetic field significantly reduces the acceleration time of ions to energies above PeV, and acceleration is possible over a short part of the orbital period. Three-dimensional flow computations were performed[1] using the relativistic MHD code PLUTO. The PLUTO code is described in [231]. In a magnetic field $\sim$ G, under typical conditions, the Ampère forces acting on the plasma exceed the Coriolis forces caused by the motion of the pulsar in a binary system and determine the local structure of the flow in the particle acceleration region. Figure 11 demonstrates a significant anisotropy of the flow along the magnetic field of the wind of a massive star. This leads to anisotropy in the angular distribution of particles. Beyond the shock termination of the pulsar wind, regions with moderately relativistic speeds (Lorentz factors $\Gamma \sim 2$–3) are observed, where high-energy protons are effectively scattered and accelerated. The anisotropic distribution of ultrarelativistic protons leads to anisotropy of gamma and neutrino radiation, which allows reconciling the possible

[1] Jointly with A E Petrov, K P Levenfish, and G A Ponomarev (see https://doi.org/10.1016/j.asr.2024.01.021).

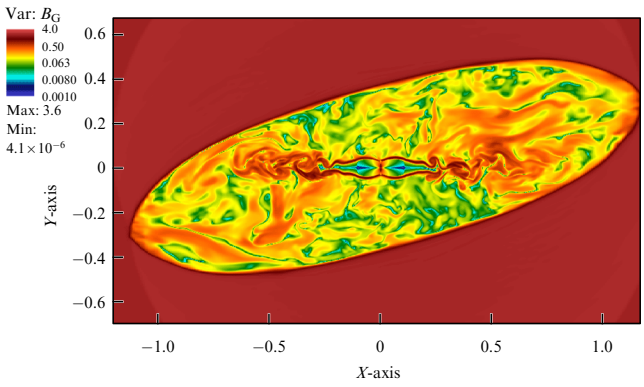

Figure 11. Structure of the magnetic field in the region of collision of relativistic wind of a pulsar with flow of magnetized wind from a massive star. Computation was performed in a three-dimensional relativistic MHD model for a pulsar with wind power $\dot{E} \sim 10^{37}$ erg s^{-1}, interacting with wind plasma of a massive star carrying a magnetic field $\sim$ G. Axial coordinates are measured in astronomical units. Strong magnetization of wind from the massive star leads to the formation of an anisotropic region of wind collision, elongated along the magnetic field of stellar wind (directed diagonally in the figure). Effective confinement of protons by a strong magnetic field in region of collision of winds and presence of regions with moderately relativistic flow velocities behind the termination shock of pulsar wind contribute to acceleration of protons to energies above PeV.

efficiency of the conversion of pulsar wind power into gamma radiation, with the characteristics of the flare detected by Carpet-2. On the other hand, emission anisotropy reduces the expected rate of the flare observations.

The model spectra of the particles shown in Fig. 9, which are accelerated in certain orbital phases in binary gamma-ray sources, allow associating the PeV photon source LHAASO J2032+4102 [214] with PSR J2032+4127/MT91 213. The photomesonic radiation mechanism discussed in [225] is of a threshold nature and requires proton energies $\gtrsim 10$ PeV. As the pulsar moves along its orbit from the perihelion, the maximum energies of the accelerated protons decrease, the photomeson process becomes ineffective, and the powerful flare terminates. However, hard spectra of protons with energies $\lesssim$ PeV can provide the energy fluxes of gamma rays observed by VERITAS, MAGIC, and LHAASO at a level of $\gtrsim 10^{-13}$ erg cm^{-2} s^{-1} after the instant of the burst due to inelastic collisions of accelerated particles with particles of the medium.

Other binary gamma-ray sources with massive companions, LS 5039, LS I+61 303, and PSR B1259−63/LS 2883, whose periods are much shorter than that of PSR J2032+4127/MT91 213, may be interesting objects for observations in the PeV-range by the LHAASO and TAIGA observatories [207] and the Cherenkov Telescope Array Observatory. The sensitivity of the TAIGA telescopes will allow searching for the emission of transient high-energy gamma-ray sources in the Galaxy. Energetic neutrinos from such sources can contribute to neutrino events observed by the Baikal-GVD [65] and IceCube [64] observatories. An analysis of high-energy neutrinos detected by the IceCube Observatory [232–234] indicates the presence of a galactic component, and binary gamma-ray sources in the Galaxy are possible candidates.

The possibility of multi-messenger observations of the radiation from galactic sources of photons and neutrinos associated with relativistic winds of pulsars and jets of accreting sources (in particular, microquasars and gamma-ray binaries) allows studying the physical processes of conversion of the flow energy into high-energy radiation, which are so clearly manifested in the phenomenon of gamma-ray bursts.

The author is grateful to A M Krassilchtchikov, K P Levenfish, A E Petrov, S M Osipov, V I Romansky, S V Troitsky, Yu A Uvarov, and D D Frederiks for the useful discussions.

References

1. Klebesadel R W, Strong I B, Olson R A *Astrophys. J.* **182** L85 (1973)
2. Mazets E P, Golenetskii S V, Il'inskii V N *JETP Lett.* **19** 77 (1974); *Pis'ma Zh. Eksp. Teor. Fiz.* **19** 126 (1974)
3. Gehrels N, Ramirez-Ruiz E, Fox D B *Annu. Rev. Astron. Astrophys.* **47** 567 (2009)
4. Mészáros P *Annu. Rev. Astron. Astrophys.* **40** 137 (2002)
5. Piran T *Rev. Mod. Phys.* **76** 1143 (2005)
6. Nava L *Int. J. Mod. Phys. D* **27** 1842003 (2018)
7. Aptekar R L et al. *Phys. Usp.* **62** 739 (2019); *Usp. Fiz. Nauk* **189** 785 (2019)
8. Mészáros P *Memorie Soc. Astron. Italiana* **90** 57 (2019)
9. Hurley K *AIP Conf. Proc.* **662** 153 (2003)
10. Mészáros P et al., arXiv:1506.02707
11. Mei A et al. *Astrophys. J.* **941** 82 (2022)
12. Frail D A et al. *Astrophys. J.* **562** L55 (2001)
13. O'Connor B et al. *Sci. Adv.* **9** eadi1405 (2023)
14. Gal-Yam A et al. *Astrophys. J.* **639** 331 (2006)
15. Ghirlanda G et al. *Astron. Astrophys.* **578** A71 (2015)
16. Huang Y-J et al. *Astrophys. J.* **897** 69 (2020)
17. Shvartzvald Y et al. *Astrophys. J.* **964** 74 (2024); arXiv:2304.14482
18. Sunyaev R et al. *Astron. Astrophys.* **656** A132 (2021)
19. Band D et al. *Astrophys. J.* **413** 281 (1993)
20. Amati L et al. *Astron. Astrophys.* **390** 81 (2002)
21. Yonetoku D et al. *Astrophys. J.* **609** 935 (2004)
22. Abdo A A et al. *Astrophys. J.* **706** L138 (2009)
23. Acciari V A et al. (MAGIC Collab.) *Nature* **575** 455 (2019)
24. Veres P et al. (MAGIC Collab.) *Nature* **575** 459 (2019)
25. Abdalla H et al. *Nature* **575** 464 (2019)
26. Abdalla H et al. (HESS Collab.). *Science* **372** 1081 (2021)
27. Ravasio M E et al. *Astron. Astrophys.* **613** A16 (2018)
28. Burgess J M et al. *Nat. Astron.* **4** 174 (2020)
29. Yassine M et al. *Astron. Astrophys.* **640** A91 (2020)
30. Li L et al. *Astrophys. J. Suppl.* **254** 35 (2021)
31. Burgess J M et al. *Astrophys. J.* **784** 17 (2014)
32. Ginzburg V L, Syrovatskii S I *Annu. Rev. Astron. Astrophys.* **3** 297 (1965)
33. Kennel C F, Coroniti F V *Astrophys. J.* **283** 694 (1984)
34. Mooley K P et al. *Nature* **561** 355 (2018)
35. Mazets E P et al. *Astrophys. Space Sci.* **80** 3 (1981)
36. Berger E *Annu. Rev. Astron. Astrophys.* **52** 43 (2014)
37. Blinnikov S I et al. *Sov. Astron. Lett.* **10** 177 (1984); *Pis'ma Astron. Zh.* **10** 422 (1984)
38. Paczynski B *Astrophys. J.* **308** L43 (1986)
39. Eichler D et al. *Nature* **340** 126 (1989)
40. Postnov K A, Yungelson L R *Living Rev. Relat.* **17** 3 (2014)
41. Gompertz B P et al. *Nat. Astron.* **7** 67 (2023)
42. Margutti R, Chornock R *Annu. Rev. Astron. Astrophys.* **59** 155 (2021)
43. Radice D, Bernuzzi S, Perego A *Annu. Rev. Nucl. Part. Sci.* **70** 95 (2020)
44. Sneppen A et al. *Nature* **614** 436 (2023)
45. Metzger B D *Living Rev. Relat.* **23** 1 (2020)
46. Blinnikov S I et al. *Astron. Rep.* **65** 385 (2021); *Astron. Zh.* **98** 379 (2021)
47. Evans P A et al. *Mon. Not. R. Astron. Soc.* **444** 250 (2014)
48. de Wet S et al. *Astron. Astrophys.* **677** A32 (2023); arXiv:2307.10339
49. Zhang B-B et al. *Astrophys. J.* **748** 132 (2012)
50. Meszaros P, Rees M J *Astrophys. J.* **405** 278 (1993)
51. Rees M J, Meszaros P *Astrophys. J.* **430** L93 (1994)
52. Tchekhovskoy A, Giannios D *Mon. Not. R. Astron. Soc.* **447** 327 (2015)

53. Duncan R C, Thompson C *Astrophys. J. Lett.* **392** L9 (1992)
54. Spruit H C, Daigne F, Drenkhahn G *Astron. Astrophys.* **369** 694 (2001)
55. Lyubarsky Y *Astrophys. J.* **698** 1570 (2009)
56. Bucciantini N et al. *Mon. Not. R. Astron. Soc.* **396** 2038 (2009)
57. Thompson C *Mon. Not. R. Astron. Soc.* **270** 480 (1994)
58. Mészáros P, Rees M J *Astrophys. J.* **530** 292 (2000)
59. Beloborodov A M, Mészáros P *Space Sci. Rev.* **207** 87 (2017)
60. Zhang B, Yan H *Astrophys. J.* **726** 90 (2011)
61. Derishev E V, Kocharovsky V V, Kocharovsky Vl V *Astrophys. J.* **521** 640 (1999)
62. Beloborodov A M *Mon. Not. R. Astron. Soc.* **407** 1033 (2010)
63. Acuner Z et al. *Astrophys. J.* **893** 128 (2020)
64. Aartsen M G et al. *JINST* **12** P03012 (2017)
65. Allakhverdyan V A et al. *Mon. Not. R. Astron. Soc.* **526** 942 (2023); arXiv:2307.07327
66. Vereshchagin G, Li L, Bégué D *Mon. Not. R. Astron. Soc.* **512** 4846 (2022)
67. Dai C Y et al. *Astrophys. J. Lett.* **957** L32 (2023); arXiv:2307.14113
68. Frederiks D et al. *Astrophys. J.* **949** L7 (2023)
69. De Angelis A et al. *Exp. Astron.* **51** 1225 (2021)
70. Bykov A M, Osipov S M, Romanovskii V I *J. Exp. Theor. Phys.* **134** 487 (2022); *Zh. Eksp. Teor. Fiz.* **161** 570 (2022)
71. Rees M J, Mészáros P *Astrophys. J. Lett.* **430** L93 (1994)
72. Daigne F, Mochkovitch R *Mon. Not. R. Astron. Soc.* **296** 275 (1998)
73. Bošnjak Ž, Daigne F *Astron. Astrophys.* **568** A45 (2014)
74. Bošnjak Ž, Barniol Duran R, Pe'er A *Galaxies* **10** (2) 38 (2022)
75. Minhajur Rahaman S, Granot J, Beniamini P *Mon. Not. R. Astron. Soc. Lett.* **528** L45 (2024); arXiv:2308.00403
76. Toma K, Wu X-F, Mészáros P *Mon. Not. R. Astron. Soc.* **415** 1663 (2011)
77. Stanek K Z et al. *Astrophys. J.* **522** L39 (1999)
78. Kobayashi S, Piran T, Sari R *Astrophys. J.* **490** 92 (1997)
79. Beniamini P, Nava L, Piran T *Mon. Not. R. Astron. Soc.* **461** 51 (2016)
80. Usov V V *Nature* **357** 472 (1992)
81. Mészáros P, Rees M J *Astrophys. J.* **482** L29 (1997)
82. Lyutikov M, Blandford R, astro-ph/0312347
83. Bykov A M et al. *Space Sci. Rev.* **173** 309 (2012)
84. Shao X, Gao H *Astrophys. J.* **927** 173 (2022)
85. Kagan D et al. *Space Sci. Rev.* **191** 545 (2015)
86. Zelenyi L M et al. *Phys. Usp.* **53** 933 (2010); *Usp. Fiz. Nauk* **180** 973 (2010)
87. Sironi L, Spitkovsky A *Astrophys. J. Lett.* **783** L21 (2014)
88. Blandford R et al. *Space Sci. Rev.* **207** 291 (2017)
89. Uzdensky D A *J. Plasma Phys.* **88** 905880114 (2022)
90. Hoshino M *Astrophys. J.* **946** 77 (2023)
91. Bykov A M, Mészáros P *Astrophys. J.* **461** L37 (1996)
92. Lemoine M, Waxman E *JCAP* **2009** (11) 009 (2009)
93. Blandford R, Meier D, Readhead A *Annu. Rev. Astron. Astrophys.* **57** 467 (2019)
94. Warren D C et al. *Mon. Not. R. Astron. Soc.* **452** 431 (2015)
95. Derishev E V et al. *Phys. Rev. D* **68** 043003 (2003)
96. Bresci V, Lemoine M, Gremillet L *Phys. Rev. Research* **5** 023194 (2023)
97. Blandford R, Eichler D *Phys. Rep.* **154** 1 (1987)
98. Berezhko E G, Krymskii G F *Sov. Phys. Usp.* **31** 27 (1988); *Usp. Fiz. Nauk* **154** 49 (1988)
99. Bykov A M, Toptygin I N *Phys. Usp.* **36** 1020 (1993); *Usp. Fiz. Nauk* **163** (11) 19 (1993)
100. Artemyev A V, Zimovets I V, Rankin R *Astron. Astrophys.* **589** A101 (2016)
101. Bykov A M *Phys. Usp.* **61** 805 (2018); *Usp. Fiz. Nauk* **188** 894 (2018)
102. Bresci V et al. *Phys. Rev. D* **106** 023028 (2022)
103. Berezinskii V S et al. *Astrophysics of Cosmic Rays* (Ed. V L Ginzburg) (Amsterdam: North-Holland, 1990); Translated from Russian: *Astrofizika Kosmicheskikh Luchei* (Ed. V L Ginzburg) (Moscow: Nauka, 1990)
104. Ptuskin V S *Phys. Usp.* **50** 534 (2007); *Usp. Fiz. Nauk* **177** 558 (2007)
105. Marcowith A et al. *Rep. Prog. Phys.* **79** 046901 (2016)
106. Bykov A M et al. *Space Sci. Rev.* **214** 41 (2018)
107. Bell A R, Matthews J H, Blundell K M *Mon. Not. R. Astron. Soc.* **488** 2466 (2019)
108. Achterberg A et al. *Mon. Not. R. Astron. Soc.* **328** 393 (2001)
109. Bykov A M, Treumann R A *Astron. Astrophys. Rev.* **19** 42 (2011)
110. Pelletier G et al. *Space Sci. Rev.* **207** 319 (2017)
111. Birdsall C K, Langdon A B *Plasma Physics via Computer Simulation* (Boca Raton, FL: CRC Press, 1991) https://doi.org/10.1201/9781315275048
112. Spitkovsky A *Astrophys. J.* **682** L5 (2008)
113. Sironi L, Spitkovsky A *Astrophys. J.* **698** 1523 (2009)
114. Sironi L, Spitkovsky A, Arons J *Astrophys. J.* **771** 54 (2013)
115. Sironi L, Spitkovsky A *Astrophys. J.* **741** 39 (2011)
116. Lu Y et al. *Astrophys. J.* **908** 147 (2021)
117. Romansky V I, Bykov A M, Osipov S M *J. Phys. Conf. Ser.* **1400** 022005 (2019)
118. Demidem C, Nättilä J, Veledina A *Astrophys. J. Lett.* **947** L10 (2023)
119. Mizuno Y et al. *Mon. Not. R. Astron. Soc.* **439** 3490 (2014)
120. Trotta D et al. *Mon. Not. R. Astron. Soc.* **525** 1856 (2023)
121. Comisso L, Sobacchi E, Sironi L *Astrophys. J.* **895** L40 (2020)
122. Comisso L, Sironi L *Phys. Rev. Lett.* **127** 255102 (2021)
123. Goto R, Asano K *Astrophys. J.* **933** 18 (2022)
124. Werner G R, Philippov A A, Uzdensky D A *Mon. Not. R. Astron. Soc.* **482** L60 (2019)
125. Zhdankin V et al. *Phys. Rev. Lett.* **118** 055103 (2017)
126. Comisso L, Sironi L *Astrophys. J.* **886** 122 (2019)
127. Arons J *Space Sci. Rev.* **173** 341 (2012)
128. Bykov A M et al. *Mon. Not. R. Astron. Soc.* **421** L67 (2012)
129. Zrake J *Astrophys. J.* **823** 39 (2016)
130. Petrosian V, Bykov A M *Space Sci. Rev.* **134** 207 (2008)
131. Lemoine M *Phys. Rev. Lett.* **129** 215101 (2022)
132. Perri S et al. *Space Sci. Rev.* **218** 26 (2022)
133. Beniamini P, Piran T *Astrophys. J.* **769** 69 (2013)
134. Ghisellini G et al. *Memorie Soc. Astron. Italiana* **93** 139 (2022)
135. Ghisellini G et al. *Astron. Astrophys.* **636** A82 (2020)
136. Sari R, Piran T, Narayan R *Astrophys. J.* **497** L17 (1998)
137. Freedman D L, Waxman E *Astrophys. J.* **547** 922 (2001)
138. Murase K et al. *Astrophys. J.* **746** 164 (2012)
139. Lemoine M *Mon. Not. R. Astron. Soc.* **453** 3772 (2015)
140. Ryde F et al. *Astrophys. J. Lett.* **932** L15 (2022)
141. Ghisellini G, Celotti A, Lazzati D *Mon. Not. R. Astron. Soc.* **313** L1 (2000)
142. Oganesyan G et al. *Astrophys. J.* **846** 137 (2017)
143. Oganesyan G et al. *Astron. Astrophys.* **628** A59 (2019)
144. Gill R, Kole M, Granot J *Galaxies* **9** (4) 82 (2021)
145. Kole M et al. *Astron. Astrophys.* **644** A124 (2020)
146. Chattopadhyay T et al. *Astrophys. J.* **936** 12 (2022)
147. Sharma V et al. *Astrophys. J.* **882** L10 (2019)
148. Burgess J M et al. *Astron. Astrophys.* **627** A105 (2019)
149. Wang H-B, Lan M-X *Astrophys. J.* **946** 12 (2023)
150. Kuwata A et al. *Astrophys. J.* **943** 118 (2023)
151. Malesani D B et al., arXiv:2302.07891
152. Pal S et al. *Atmosphere* **14** (2) 217 (2023)
153. Abbasi R et al. *Astrophys. J. Lett.* **946** L26 (2023)
154. Blanchard P K et al., arXiv:2308.14197
155. Williams M A et al. *Astrophys. J. Lett.* **946** L24 (2023)
156. Ravasio M A et al., arXiv:2303.16223
157. Pe'er A, Waxman E *Astrophys. J.* **613** 448 (2004)
158. Krassilchtchikov A M et al. *J. Phys. Conf. Ser.* **1400** 022031 (2019)
159. Tomsick J A et al. *PoS* **ICRC2023** 745 (2023) https://doi.org/10.22323/1.444.0745; arXiv:2308.12362
160. Tatischeff V et al. *Memorie Soc. Astron. Italiana* **90** 137 (2019)
161. Laskar T et al. *Astrophys. J. Lett.* **946** L23 (2023)
162. Negro M et al. *Astrophys. J. Lett.* **946** L21 (2023)
163. Huang Y et al., GRB Coordinates Network, Circular Service (32677) 1 (2022)
164. Dzhappuev D D et al., The Astronomer's Telegram No. 15669 (2022) p. 1
165. Cao Z et al. (LHAASO Collab.) *Science* **380** 1390 (2023)
166. Zhang B T et al. *Astrophys. J. Lett.* **947** L14 (2023)
167. Isravel H, Bégué D, Pe'er A *Astrophys. J.* **956** 12 (2023)
168. Troitsky S V *JETP Lett.* **116** 767 (2022); *Pis'ma Zh. Eksp. Teor. Fiz.* **116** 745 (2022)

169. Troitsky S *JCAP* **2024** (01) 016 (2024); arXiv:2307.08313
170. Mazets E P et al. *Nature* **282** 587 (1979)
171. Ridnaia A et al. *Nat. Astron.* **5** 372 (2021)
172. Popov S B, Postnov K A, in *Evolution of Cosmic Objects through their Physical Activity, Proc. of the Conf. Dedicated to Viktor Ambartsumian's 100th Anniversary, 15–18 September 2008, Yerevan, Byurakan, Armenia* (Eds H A Harutyunian, A M Mickaelian, Y Terzian) (Yerevan: Gitutyun, 2010) p. 129
173. Cordes J M, Chatterjee S *Annu. Rev. Astron. Astrophys.* **57** 417 (2019)
174. Lyubarsky Yu *Astrophys. J.* **897** 1 (2020)
175. Beloborodov A M *Astrophys. J. Lett.* **922** L7 (2021)
176. Raymond J C *Space Sci. Rev.* **214** 28 (2018)
177. Margutti R et al. *Astrophys. J.* **797** 107 (2014)
178. Tan J C, Matzner C D, McKee C F *Astrophys. J.* **551** 946 (2001)
179. Lazzati D et al. *Astrophys. J.* **750** 68 (2012)
180. Gottlieb O, Tchekhovskoy A, Margutti R *Mon. Not. R. Astron. Soc.* **513** 3810 (2022)
181. Bykov A, Romansky V, Osipov S *Universe* **8** (1) 32 (2022)
182. Bykov A M et al. *Space Sci. Rev.* **214** 41 (2018)
183. Margutti R et al. *Astrophys. J.* **872** 18 (2019)
184. Bright J S et al. *Astrophys. J.* **926** 112 (2022)
185. Metzger B D *Astrophys. J.* **932** 84 (2022)
186. Sun N-C et al. *Mon. Not. R. Astron. Soc.* **519** 3785 (2023)
187. Shustov B M *Astrophysics* **64** 405 (2021); *Astrofizika* **64** 455 (2021)
188. Amato E, arXiv:2001.04442
189. Coroniti F V *Astrophys. J.* **349** 538 (1990)
190. Aharonian F A, Bogovalov S V, Khangulyan D *Nature* **482** 507 (2012)
191. Beskin V S *Phys. Usp.* **40** 659 (1997); *Usp. Fiz. Nauk* **167** 689 (1997)
192. Porth O, Komissarov S S, Keppens R *Mon. Not. R. Astron. Soc.* **438** 278 (2014)
193. Tchekhovskoy A, Philippov A, Spitkovsky A *Mon. Not. R. Astron. Soc.* **457** 3384 (2016)
194. Bühler R, Giomi M *Mon. Not. R. Astron. Soc.* **462** 2762 (2016)
195. Levenfish K P et al. *J. Phys. Conf. Ser.* **2103** 012020 (2021)
196. Gaensler B M, Slane P O *Annu. Rev. Astron. Astrophys.* **44** 17 (2006)
197. Kargaltsev O, Pavlov G G *AIP Conf. Proc.* **983** 171 (2008)
198. Kargaltsev O et al. *J. Plasma Phys.* **83** 635830501 (2017)
199. Tavani M et al. *Science* **331** 736 (2011)
200. Abdo A A et al. *Science* **331** 739 (2011)
201. Bühler R, Blandford R *Rep. Prog. Phys.* **77** 066901 (2014)
202. Pshirkov M S et al. *Mon. Not. R. Astron. Soc.* **496** 5227 (2020)
203. Porth O et al. *Space Sci. Rev.* **207** 137 (2017)
204. Guilbert P W, Fabian A C, Rees M J *Mon. Not. R. Astron. Soc.* **205** 593 (1983)
205. Cerutti B, Uzdensky D A, Begelman M C *Astrophys. J.* **746** 148 (2012)
206. Cao Z et al. (Lhaaso Collab.) *Science* **373** 425 (2021)
207. Kuzmichev L A et al. *Phys. Atom. Nucl.* **84** 966 (2021)
208. Dzhappuev D D et al. *Astrophys. J. Lett.* **916** L22 (2021)
209. Ackermann M et al. *Science* **334** 1103 (2011)
210. Aharonian F et al. *Astron. Astrophys.* **431** 197 (2005)
211. Abdo A A et al. *Astrophys. J.* **658** L33 (2007)
212. Abeysekara A U et al. *Astrophys. J.* **861** 134 (2018)
213. Amenomori M et al. (Tibet AS_γ Collab.) *Phys. Rev. Lett.* **127** 031102 (2021)
214. Cao Z et al. *Nature* **594** 33 (2021)
215. Abeysekara A U et al. *Nat. Astron.* **5** 465 (2021)
216. Bykov A M *Astron. Astrophys. Rev.* **22** 77 (2014)
217. Aharonian F, Yang R, de Oña Wilhelmi E *Nat. Astron.* **3** 561 (2019)
218. Bykov A M, Kalyashova M E *Adv. Space Res.* **70** 2685 (2022)
219. Ginzburg V L, Dogel' V A *Sov. Phys. Usp.* **32** 385 (1989); *Usp. Fiz. Nauk* **158** 3 (1989)
220. Abdo A A et al. (Fermi LAT Collab.) *Science* **326** 1512 (2009)
221. Antokhin I I et al. *Astrophys. J.* **926** 123 (2022)
222. Mioduszewski A J et al. *Astrophys. J.* **553** 766 (2001)
223. Koljonen K I I et al. *Mon. Not. R. Astron. Soc.* **524** L89 (2023)
224. Aleksić J et al. *Astrophys. J.* **721** 843 (2010)
225. Bykov A M et al. *Astrophys. J. Lett.* **921** L10 (2021)
226. Ho W C G et al. *Mon. Not. R. Astron. Soc.* **464** 1211 (2017)
227. Takata J et al. *Astrophys. J.* **836** 241 (2017)
228. Abeysekara A U et al. *Astrophys. J. Lett.* **867** L19 (2018)
229. Ng C-Y et al. *Astrophys. J.* **880** 147 (2019)
230. Bykov A M, Gladilin P E, Osipov S M *Mon. Not. R. Astron. Soc.* **429** 2755 (2013)
231. Mignone A et al. *Astrophys. J. Suppl.* **170** 228 (2007)
232. Neronov A, Semikoz D *Astropart. Phys.* **75** 60 (2016)
233. Troitsky S V *Phys. Usp.* **64** 1261 (2021); *Usp. Fiz. Nauk* **191** 1333 (2021)
234. Kovalev Y Y, Plavin A V, Troitsky S V *Astrophys. J. Lett.* **940** L41 (2022)